SSRG International Journal of Civil Engineering
ISSN: 2348-8352/ https://doi.org/10.14445/23488352/IJCE-V13I3P106

Volume 13 Issue 3, 71-92, March 2026

Original Article

Comparative Analysis of Ant Colony and Whale Optimization Algorithms for Hyperparameter Optimization in RNN-Based Constitutive Modeling of Unstabilized Rammed Earth

Chaymae Salhi[1], Mouna El Mkhalet[2], Nouzha Lamdouar[3]

[1,2,3]*Civil Engineering and Construction structure GCC laboratory, Mohammadia School of Engineers EMI, Mohammed V University, Rabat, Morocco.*

[1]*Corresponding Author : chaymae.salhi@research.emi.ac.ma*

Received: 07 December 2025 Revised: 08 January 2026 Accepted: 07 February 2026 Published: 23 March 2026

Abstract - *The goal of this research is to develop an accurate predictive model for the stress-strain behavior of unstabilized rammed earth in compression using Recurrent Neural Networks (RNNs), where the hyperparameters are determined using Ant Colony Optimization (ACO) and Whale Optimization Algorithm (WOA). Written in Python, the NNs were trained on synthetic data consisting of 2,000 random stress-strain curves generated from probabilistic distributions of peak strain and strength. Experiments show the effectiveness of metaheuristic search: although a manually tuned baseline mean squared error of 0.00049, a two-hand (Ant Colony Optimization and Whale Optimization Algorithm) optimized model drastically outperformed prediction performance with convergence to 0.000064 and 0.000039 in terms of Mean Squared Error (MSE), respectively. The reliability of the model was demonstrated by experimental validation with various types of soil mixtures.*

Keywords - *Unstabilized Rammed Earth, Recurrent Neural Networks, Ant Colony Optimization, Whale Optimization Algorithm, Compression Stress.*

1. Introduction

1.1. Overview of Rammed Earth

The construction sector is recognized as one of the most environmentally impactful industries. According to Maskell et al. [1], buildings are associated with one-third of the global energy-related emissions. In addition, existing building materials are based on manufacturing technology and industrial elements with a high energy content, as well as greenhouse gas (mainly CO2) emissions [2]. Thus, the current world trends in stepping closer toward sustainable development have steered attention to alternative energy-efficient buildings [3].

Rammed Earth (RE) seems to be among the most interesting and promising low-carbon construction materials, mainly due to its very poor environmental impact (conditional value 0.023 kg-eqCO2/kg), compared to standard building materials such as concrete (0.130 kg-eqCO2/kg) [4]. Besides low emissions, RE has practical advantages due to its affordability, utilization of local aggregates, recyclability, and favorable thermal performance with good adequate regulation capacities [5]. The technique is an early method of construction, which involves placing moist earth into a temporary framework to obtain the desired wall height. Usually, the soil mixture consists of well-graded sand or clayey sand; when clay is the only binder involved, it is called Unstabilized Rammed Earth (URE), and with other additives like cement or lime, the material is classified as Stabilized Rammed Earth (SRE) [6].

However, it shows many differences as far as variability in its physical properties and displays a non-linear mechanical behavior [7]. The mechanical characteristics of RE, in particular the compressive strength, Young's modulus, and peak strain, suffer from a considerable scatter compared to common conventional materials, such as, for instance, concrete or steel. [8]. In addition, the material exhibits non-linear stress-strain behavior that is difficult to simulate with deterministic models, although it is crucial for a faithful structural analysis [9].

This variability creates a fundamental challenge for reliable structural design, since conventional deterministic

constitutive models fail to adequately represent the accurate mechanical response of URE.

To address the inherent uncertainties, probabilistic design and reliability analysis are increasingly adopted in modern structural engineering, which have the advantage of the use of a series of material relation databases to cover material behavior facing specific treatment for characteristics as random variables in order to better reflect physical reality. However, there are few studies adopting a reliability-based approach to RE construction specifically. As an example of these few studies, the paper of Kianfar and Toufigh [10], where a reliability analysis was conducted for URE and cement-stabilized RE walls when both load effects and material resistances were considered as random variables. However, this research is oriented to the reliability of the structure level and less on developing predictive constitutive models that are able to predict material performance at the stress-strain level.

The stress-strain curve is an essential characteristic used to describe the mechanical properties of materials such as RE, and a necessary data source for structural design [11, 12]. For a natural material like RE, compressive strength is one of the key parameters in determining material mechanical characteristics and bearing capacity [13]. Therefore, some studies have investigated the compressive performance of RE by means of laboratory tests in recent years [8] with a focus on both URE and SRE.

For URE, Gil-Martín et al. [14] performed uniaxial compression tests and announced the stress-strain curves based on experimental results, but did not present a general analytical expression. Similarly, Ávila et al. presented both the compressive and shear response of URE with full stress-strain curves and a constitutive model fitted on test results, but without proposing one single familiar formula. Bui et al. [16] pointed out the sensitivity of URE's compressive strength to moisture content. In contrast, Maniatidis and Walker [17] tested URE walls and specimens in order to determine the compressive strength and stiffness, and stress–strain curves were obtained. However, they were based on empirical interpretation without formulating a unified model.

The application of reinforcing and stabilizing agents of SRE in enhancing the strength property seems to be becoming a trend in construction [8]. El Bourki et al. [18] investigated date palm fiber reinforcement and reported the obtained stress-strain curves from compression, albeit also without providing the generalized equation. Raavi and Tripura [19] studied cement-stabilized rammed earth wallettes having coir fibers, bamboo splints, and steel bars as reinforcement, reporting enhancement of compressive and shear performance with stress-strain curves but with no analytic foundation. Likewise, Ávila et al. [20] also worked on lime-stabilized RE and observed the influence of different levels of lime contents and curing periods on the development of compressive strength, although a generalized stress-strain expression was not provided despite the fact that they displayed stress-strain curves from unconfined compression tests.

Several other studies, including the ones by Miccoli et al. [21] and Naseri et al. [22], have recently re-emphasized the need for stress-strain curves to explore the mechanical response of RE under compression and demonstrated how variables such as fiber reinforcement or slag stabilization influence stiffness, ductility, and failure modes.

However, all of these contributions are often limited to each case, so that only experimental findings with a particular type of soil/stabilizer are available instead of analytical expressions that can be applied generally as specified by Koutous and Hilali [23]. To address these limitations, Koutous and Hilali [23] suggested a form of the compressive stress-strain law for RE that is valid for the ascending part of the stress-strain curve. While of great interest, such analytical constructs involve algebraic expressions and are not adaptive with respect to data, making it challenging to model the stochastic and nonlinear nature characteristic of URE.

Based on this statement, although empirical relations constitute a description of the RE stress-strain performance under compression, they are only algebraic in nature and cannot learn patterns from data. On the contrary, Machine Learning, or more precisely Deep Learning, offers a great alternative to develop efficient and powerful surrogate models that can account for these complex non-linear behaviors [24, 25]. Of the many Deep Learning architectures, RNNs are especially well-suited for this type of problem. As stress-strain curves are essentially sequential data (stress state evolves as a function of strain history), RNNs can take advantage of their internal memory mechanisms to better deduce the behavior of materials than standard feedforward networks [26]. However, to the best of the authors' knowledge, there is no prior work that makes use of RNN-based models for the constitutive modeling of RE materials.

The performance of an RNN is primarily determined by its architecture and settings (Hyperparameters), such as hidden units, network depth, learning rate, and batch size [27]. Optimizing the choice of these hyperparameters is a non-trivial problem. Conventional methods often require manual configuration, i.e., the trial-and-error tuning that introduces computational redundancy and sub-optimal convergence [27].

Furthermore, there is currently no generally accepted systematic methodology for determining an optimal neural network architecture [28]. This challenge is particularly critical for modelling URE, where material nonlinearity and uncertainty demand highly optimized learning architectures.

1.2. Research Gap

To fill these gaps in the literature, this paper aims to predict the stress-strain behavior of RE under compression, especially URE. In order to address the downside of manual configuration, this work involves the utilization of metaheuristic optimization techniques in designing the RNN. Motivated by the mechanisms in nature, metaheuristic algorithms can explore complex and multi-dimensional spaces where global optima may exist [29]. The present work will focus on two approaches: Ant Colony Optimization (ACO), mimicking ants' foraging behavior, and Whale Optimization Algorithm (WOA), inspired by the hunting mechanism of the humpback whale. This, to the best of the authors' knowledge, is the first work that utilizes metaheuristic optimization algorithms for deep-learning-based constitutive modelling of URE.

In comparison to existing studies, this work contributes to the current understanding of material modelling. The experimental studies on RE bring meaningful insight into its performance under compression but display limitations in terms of soil composition and testing conditions, limiting their applicability. The propose analytical constitutive model form of Koutous and Hilali [23], underpinning the current study, provides a general representation of the URE ascending branch stress-strain curve.

However, it is deterministic, parameter-based based and does not include random variability or data-driven learning. Reliability-based works, like Kianfar and Toufigh [10], include probability-based concepts at the structural level; however, they are based on predefined material models rather than attempting to characterize the constitutive stress-strain response.

On top of the Koutous and Hilali [23] formulation, this study expands the understanding of URE behavior by turning this analytical linkage into a probabilistic data-driven framework supported by RNNs and improving prediction performance through network architecture metaheuristic optimization.

1.3. Research Novelty

The novelty of this work lies in its threefold contributions: (1) the first instance of applying RNNs to forecast compressive stress-strain behaviour of URE; (2) the first case where ACO and WOA co-function for the optimization of the hyperparameters of neural networks in earth construction materials; and (3) a deliberate inclusion of probabilistic fluctuations in influential mechanical parameters, observing that with data-driven constitutive models that capture natural stochasticity within URE.

The main aim of this paper is to advance URE structures by applying RNN-based prediction for the material behavior under compression. A second goal is to assess and compare the advantages of applying metaheuristic optimization for URE constitutive modelling while incorporating explicitly stochastic properties such as compressive strength and peak strain. In order to get this done, a comparative study of the following 3 steps is performed: (1) The first step is manually creating the Baseline RNN, (2) applying ACO for optimization of RNN hyperparameters, and (3) employing WOA for optimizing the RNN's hyperparameters. The Mean Squared Error (MSE) is used as a primary measure to assess and compare the predictive accuracy of all models. The models are based on a synthetically-generated dataset of 2,000 stress-strain curves, computed from the constitutive model for URE presented by Koutous and Hilali [23] and established probabilistic distributions. At last, in order to analyze the practical reliability and numerical stability of the models, four types of experimental formulations (Raw Earth, Sand-Earth, Rounded Gravel-Earth, and Angular Gravel-Earth) were taken as experimental validation formulations for checking the models' predictive fidelity and stability.

2. Methods

2.1. Overview and Model Definition

The core of this research is to develop and optimize an RNN model capable of accurately predicting the non-linear stress-strain relationship of URE. The model's task is to predict the 9-step stress (σ) sequence after being fed a 9-step input sequence containing the strain (ε), compressive strength (f_c), and peak strain (ε_p) at each step. By leveraging the sequential processing capabilities of RNNs, the model aims to capture the path-dependent mechanical behavior of the material under compression.

2.2. Data Generation and Computational Framework

The computational framework for this study was developed using the Python programming environment within the PyCharm IDE, utilizing the TensorFlow and Keras libraries for deep learning implementation. To train the model, a synthetic dataset was generated to simulate the stochastic mechanical behavior of URE.

Key mechanical properties were modeled as random variables based on established statistical distributions to reflect real-world material variability:

- Compressive Strength (f_c): Modeled using a Lognormal distribution with a mean value of 1.75 MPa and a Coefficient of Variation (COV) of 35%.
- Peak Strain (ε_p): Modeled using a Normal distribution with a mean of 1.9% and a standard deviation of 0.8%.

These probabilistic inputs were employed to generate 2,000 unique constitutive curves based on the analytical model introduced by Koutous and Hilali [23]. The present

constitutive law specifically represents the non-linear stress-strain behaviour of URE under compression loads, which covers only the ascending part of the stress-strain curve until failure. The temporal development of stresses was divided into a step-by-step 9-level loading procedure, which was accepted for different axial strains (0.3%, 0.5%, 0.8%, 1.0%, 1.5%, 2.0%, 2.5% and 3%). This repetitive perspective on incremental deformation allows the RNN to model the evolution of nonlinear constitutive response, depending on the accumulated strain.

2.3. Optimization Strategy

For a more rigorous measurement of the merits of metaheuristic optimization, a three-step comparative testing framework was used. The data set of 2000 stress-strain responses was split once into a training set of size 1,600 (80%) and a test set of size 400 (20%), making sure that all three procedures are trained on the same material to allow fair comparison.

These three phases of experimentation are intended to contrast the manually designed baseline model with models found using two different metaheuristics, i.e., Ant Colony Optimization (ACO) based and Whale Optimization Algorithm (WOA) based optimized models. In the optimization stage, both algorithms are implemented as a population of 10 agents (ants or whales) traversing 10 generations. This setting leads to an intense exploration of the solution space since it allows for the evaluation of 100 different hyper-parameter combinations for each algorithm out of 324 potential combinations. The difference between the stages is the hyperparameter selection strategy, as detailed in Table 1.

2.4. Validation Strategy

To verify the practical stability of the proposed models, experimental verification is conducted on the optimized RNN-ACO and RNN-WOA schemes. This step implemented 4 different material formulations—Raw Earth, Sand-Earth, Rounded Gravel-Earth, and Angular Gravel-Earth —based on the article of Koutous and Hilali [23], in order to analyse the predictive fidelity across varying soil compositions and an assorted range of mechanical properties. This shift between computational training and scenario-based validation is key to attesting the models' reliability for practical engineering purposes.

3. Results

3.1. Literature Review

3.1.1. Recurrent Neural Networks

RNNs address key limitations of conventional neural networks (CNNs) by enabling temporal modeling through architectural feedback mechanisms. Artificial Neural Networks (ANNs) are broadly categorized into two main types: feedforward neural networks and recurrent neural networks [30].

Table 1. Hyperparameter configuration for baseline and optimized models

	Stage 1	**Stage 2**	**Stage 3**
Model Settings	**Baseline RNN (Manual Selection)**	**RNN-ACO (Search Space)**	**RNN-WOA (Search Space)**
Cell Type	SimpleRNN (Fixed)	SimpleRNN (Fixed)	SimpleRNN (Fixed)
Units	50	[6, 32, 50, 64]	[6, 32, 50, 64]
Layers	1	[1, 2, 3]	[1, 2, 3]
Optimizer	Adam	['Adam', 'RMSprop', 'SGD']	['Adam', 'RMSprop', 'SGD']
Batch Size	32	[16, 32, 64]	[16, 32, 64]
Epochs	50	[50, 100, 150]	[50, 100, 150]

Conventional Neural Networks (CNN) operate under the assumption that inputs and outputs are mutually independent, an assumption that often fails in real-world problems involving sequential or time-dependent data [26, 31]. This is where RNNs become essential. Designed to process sequences and time-series data, RNNs enhance classical ANNs by incorporating recurrent connections that enable the network to maintain a hidden state-a key feature whose activation evolves-allowing the model to capture temporal dependencies in the input data [26, 32, 33]. These temporal dependencies in RNN are modeled by sharing the same weights and biases across time steps, which reduces the number of parameters and enables the network to retain information from previous steps by feeding each output back into the network as input for the next hidden layer.

RNNs are distinct from single-layer or multilayer feedforward networks in that they incorporate at least one feedback loop [34]. In its simplest form, an RNN consists of a single layer of neurons where the output at each time step is reused as input in the next, creating a temporal connection across the sequence [30]. The basic structure of an RNN is illustrated in Figure 1, based on the study by Shajun Nisha et al. [26], while a flowchart illustrating its functioning is presented in Figure 2.

RNNs can be used for both classification and regression tasks [35]. The definitions that follow are adapted from [36], who provide a foundational overview of classification and regression in the context of statistical learning.

Classification refers to tasks where the goal is to assign inputs to predefined categories or classes based on learned patterns. In machine learning, this involves training a model on labeled data so that it can predict the appropriate category for new, unseen data. Regression, on the other hand, involves predicting a continuous numerical value by modeling the relationship between one dependent variable and one or more independent variables. Common types include linear and multiple regression, depending on the number of predictors involved.

RNNs, along with their various extensions, are widely used in everyday applications such as speech recognition, image captioning, machine translation, and music generation [37]. Owing to their ability to model sequential data, RNNs have gained traction across numerous disciplines, including the engineering sector—particularly civil engineering, which has increasingly adopted RNN-based models across various subfields [37], as illustrated through several representative studies presented in the following section.

In the area of concrete material behavior, hybrid RNN–LSTM models have been employed to predict the mechanical performance of basalt fiber concrete subjected to freeze–thaw cycles, enhanced by integrating thermodynamic modeling and damage mechanics [38]. Similarly, deep RNNs with attention mechanisms have been successfully applied to the recognition of concrete microcracks under fluorescent excitation, significantly improving detection accuracy compared to conventional image processing methods [39]. In geotechnical engineering, RNNs combined with wavelet transforms and metaheuristic optimization algorithms have been developed to predict the seismic response of slope–pile–anchor reinforcement systems, demonstrating robust time-series forecasting capabilities under complex subsurface conditions [40].

Within structural health monitoring and seismic analysis, physics-informed RNN models—such as Bayesian and Runge–Kutta-based architectures—have been applied to predict structural responses under dynamic loading, offering improvements in accuracy, robustness, and uncertainty quantification [37, 41]. Furthermore, physically recurrent Neural Networks have been explored as surrogate models for multiscale material simulations, successfully capturing rate- and path-dependent behavior in heterogeneous composites under large strains [42].

Together, these studies underscore the increasing use of RNNs for classification, regression, and time-series prediction tasks across a range of civil engineering applications, including materials science, geotechnics, structural dynamics, and damage detection.

In the context of rammed-earth construction, the

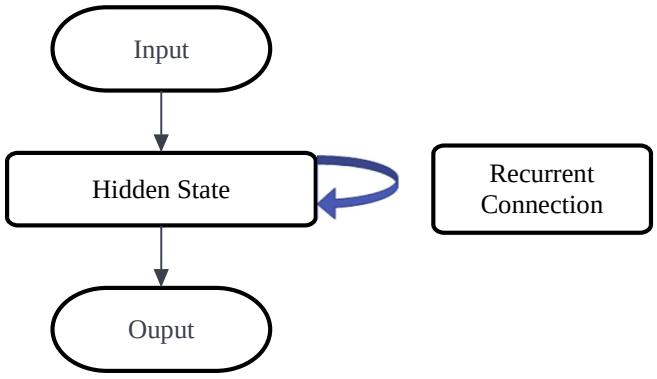

Fig. 1 Basic structure of recurrent neural networks (figure based on the study by Shajun Nisha et al. [26])

The application of soft computing methods remains limited, with notable gaps in the literature concerning the use of Machine Learning Techniques [43]. While several studies have employed models such as ANNs and Convolutional Neural Networks (CNNs) to investigate various properties of rammed earth [44-47], to the best of the authors ' knowledge, no study to date has explored the use of RNN for this purpose.

3.1.2. Ant Colony Optimization

Initially developed by Dorigo in the early 1990s, ACO is a metaheuristic technique inspired by ant behavior [48, 49]. It is based on how ants find the shortest path to a food source by depositing pheromones along the ground, which other ants detect and follow [50]. Through this process, ants progressively identify the most efficient route between their nest and the food source, effectively determining an optimal path [51]. ACO builds on this natural process by mimicking it algorithmically to solve complex optimization problems [50].

According to a bibliometric analysis by Blum [52], the majority of ACO research publications are centered in computer science, followed by engineering and mathematics. Other disciplines, such as decision sciences, physics and astronomy, and materials science, also contribute to the expanding body of ACO research, albeit to a lesser extent [52].

In civil engineering, ACO has been increasingly applied in recent years. One study utilized genetic algorithms alongside ACO to optimize non-linear wave paths for ultrasonic tomography in concrete, enhancing tomographic image generation [53]. To balance structural performance, cost, and carbon emissions, another research applied multi-objective optimization with an

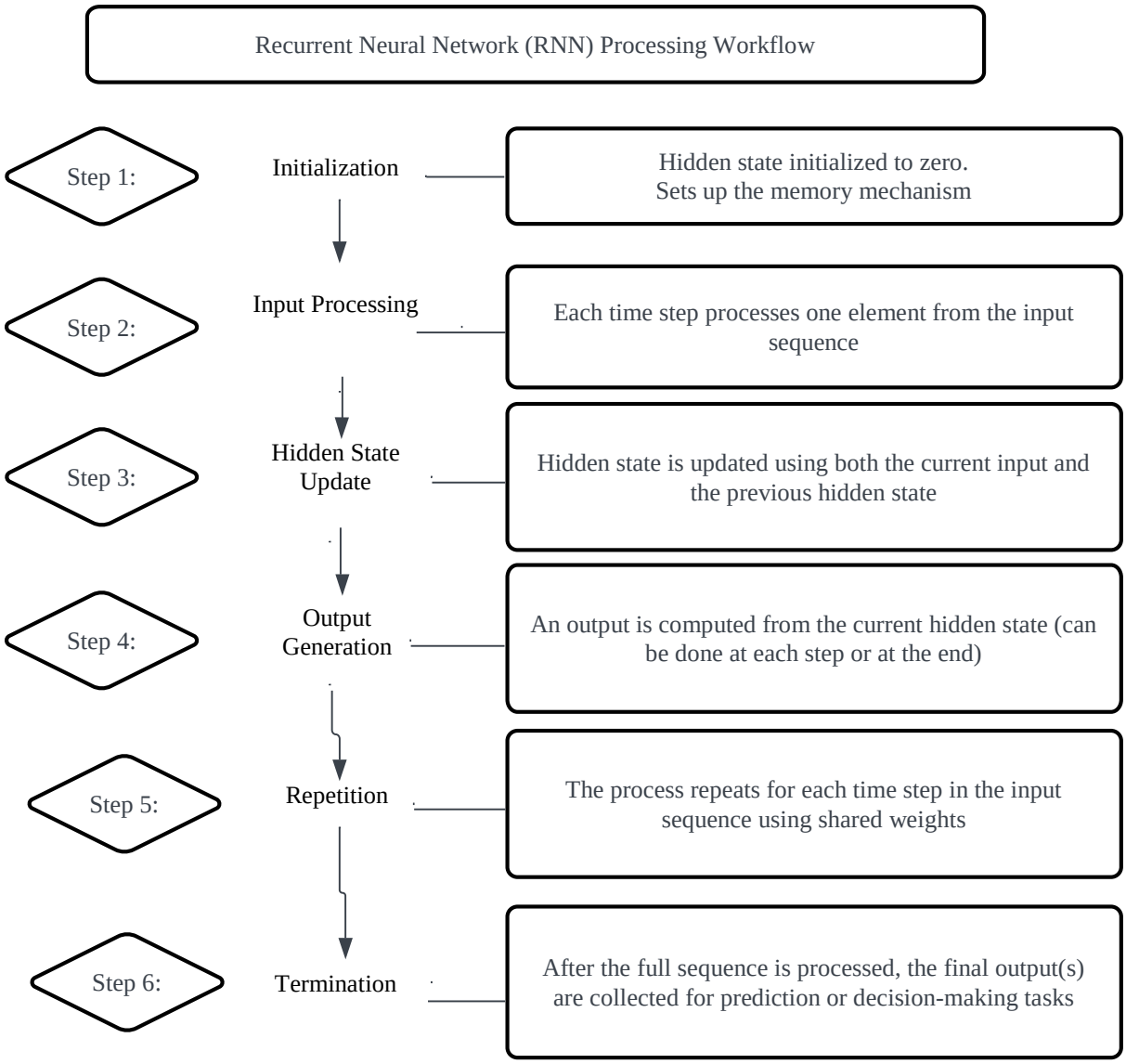

Fig. 2 Operational workflow of a recurrent neural network (flowchart based on the steps in the study by Shajun Nisha et al. [25])

Improved ACO algorithm to design steel-concrete composite columns [54].

The development of hybrid airline networks has also benefited from ACO, with optimized route and frequency settings achieved through a self-regulated algorithm [55]. Furthermore, an ant-colony-based control method was introduced to coordinate multiple MR dampers, effectively reducing vibrations in spatially irregular structures [56]. Enhancing railway planning, a metaheuristic-based multistage framework was devised to improve system cost, environmental, and socio-economic outcomes [57].

In power transmission, an ACO-based approach reduced routing costs by about 25% compared to existing methods [58]. The lateral strength of reinforced concrete columns under cyclic loading was more accurately predicted using an ACO-enhanced XGBoost model [59]. Addressing 2D pipe routing challenges, a dynamic adaptive ACO algorithm with enhanced pheromone and transfer strategies was proposed [60]. For dynamic fire evacuation planning, an improved ACO algorithm incorporated real-time fire conditions to ensure safer evacuation routes [61].

To the authors' knowledge, no study has yet explored the application of ACO for rammed earth construction in any capacity.

Figure 3 presents a flowchart summarizing the main steps of the ACO algorithm, adapted from the works of Dorigo et al. [62] and Blum [63].

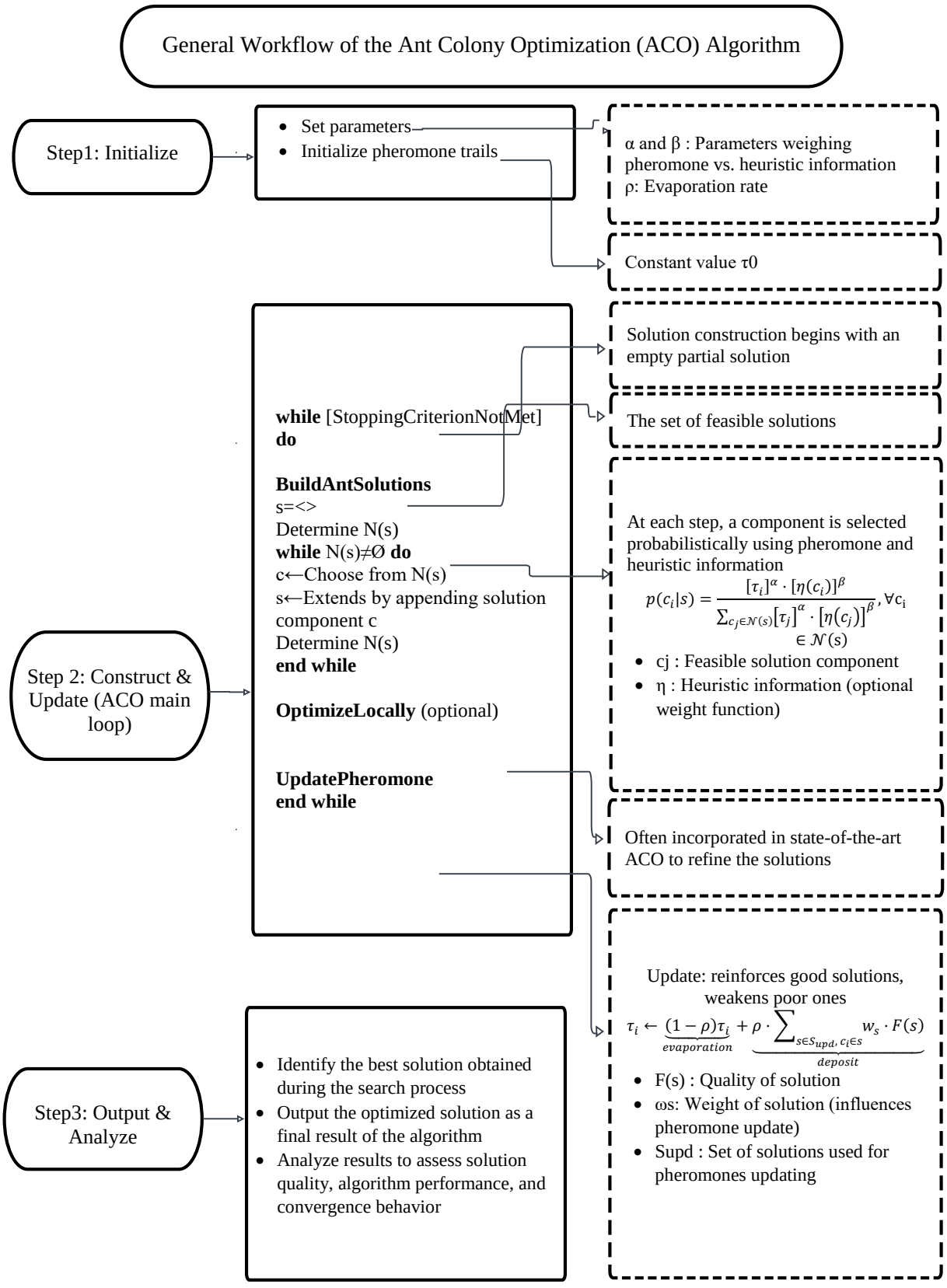

Fig. 3 General workflow of the Ant Colony Optimization (ACO) Algorithm adapted from Dorigo et al. [62] and Blum [63]

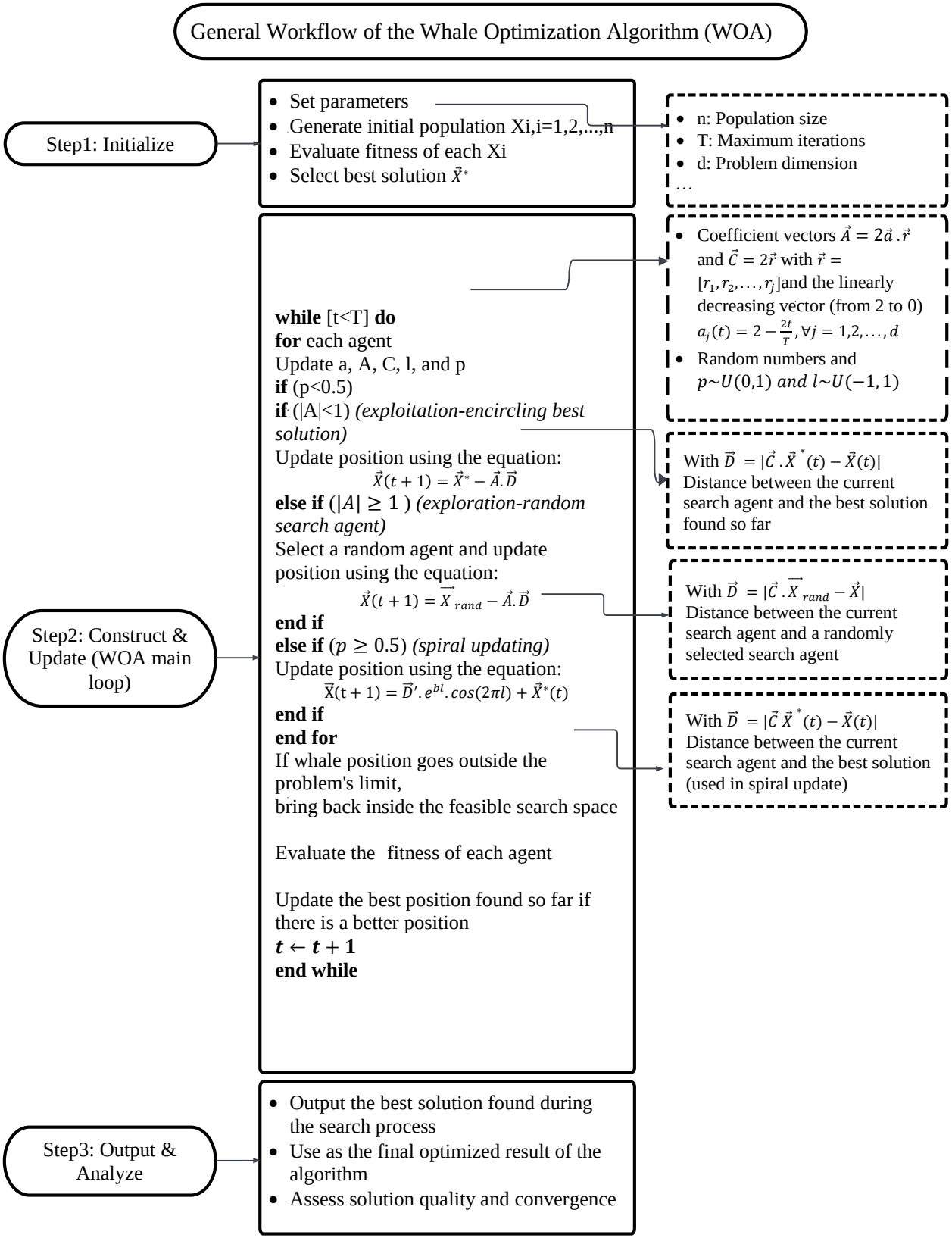

Fig. 4 General workflow of the Whale Optimization Algorithm (WOA) adapted from Gharehchopogh and Gholizadeh [76] and Mirjalilia and Lewis [64]

3.1.3. Whale Optimization Algorithm

The WOA, introduced by Mirjalili et al. in 2016 [64], is a nature-inspired metaheuristic technique based on the cooperative hunting strategy of humpback whales [65]. The algorithm models three main behaviors observed in nature: encircling prey, bubble-net feeding, and prey search [65]. In the computational framework, a population of whales represents candidate solutions to the optimization problem [66]. The WOA has been successfully applied across a wide range of disciplines, including computer science [67-69], physics and astronomy [70-72], and the energy sector [73-75]. Beyond these domains, WOA has also proven effective in supporting diverse engineering optimization problems [76].

According to Gharehchopogh and Gholizadeh [76], the engineering applications of WOA can be broadly categorized into several areas: electrical engineering, civil engineering, classification, clustering, image processing, mechanical engineering, control engineering, robotic path planning, networks, industrial engineering, task scheduling, and other engineering-related problems.

Within civil engineering, several notable contributions demonstrate the practical value of WOA. Monteiro et al. [77] introduced a vibration-based damage detection method that uses WOA to identify, locate, and quantify structural damage. Rohani et al. [78] presented one of the earliest civil engineering applications of WOA, employing it to optimize construction site workflow and thereby improve efficiency and reduce project costs. Ezzeldin and Djebedjian [79] used the WOA metaheuristic to choose pipe diameters for a network, with a rounding strategy to handle the discrete set of available pipe sizes in order to solve the classic civil task of least-cost water distribution design. Lai et al. [80] investigated hydropower reservoir operation and demonstrated that WOA achieved favorable results compared with both a Levy-flight-enhanced variant and the Harris Hawks Optimization algorithm. Finally, Brito and Miguel [81] applied WOA to the structural optimization of a multi-story reinforced concrete frame subjected to wind loads, successfully reducing material use while meeting performance constraints.

Figure 4 presents a flowchart summarizing the main steps of the WOA, adapted from the works of Gharehchopogh and Gholizadeh [76] and Mirjalili and Lewis [64].

3.2. Hyperparameter Optimization Framework

For the quantitative performance comparison of our optimization methods, the baseline model, and then both ACO and WOA were assigned to minimize the same objective function (MSE). Where fixed parameters were used for the baseline model, ACO and WOA algorithms used the same search space, as shown in Table 2. Such a consistency ensures that any slight difference in final model fitness can be directly attributed to the search performance of the meta-heuristic algorithm.

The optimization problem is defined by three elements: the decision variables, which specify the architecture of an RNN in terms of input/output connections; the objective function, which encapsulates the model's predictive performance; and the system constraints that delimit the search space. These common elements of the two algorithms are described in the subsequent sections.

3.2.1. Baseline Model

For the baseline phase, the study establishes a benchmark using a manually configured SimpleRNN to model the stress-strain behavior of URE. This model is based on a fixed decision vector h={50,1, Adam,32,50} which is consistent with the 50 hidden units, 1 recurrent layer using Adam as optimizer with a batch size of 32 and training for 50 epochs. It aims to reduce the difference between experimental stress and model predictions with MSE as a loss function:

$$Minimize\ J(h) = \frac{1}{N}\sum_{i=1}^{N}(y_i - \hat{y}_i(h))^2 \quad (1)$$

Where:

- y_i represents the actual experimental stress value.
- $\hat{y}_i(h)$is the stress value predicted by the RNN configured with hyperparameters h.
- N is the total number of samples in the validation set.

3.2.2. Optimized Models

The structure and training dynamics from the RNN are determined by a set of hyperparameters, which are considered as decision variables for the metaheuristic search. We denote it as a decision vector $h = \{u, L, o, B, E\}$. These search spaces from ACO and WOA are searched in an orderly manner to find the best configuration for modeling the stress-strain of rammed earth.

In order to find a trade-off between computational efficiency and model accuracy, discrete domains were created for each variable. These intervals describe the optimization problem bounds, as seen in Table 2.

RNN-ACO Implementation

The control parameters adopted for the ACO in this study are summarized in Table 3. The ACO search is formulated as a constrained optimization problem, in which the objective functions in Equation 1 are minimized under the hyperparameter bounds specified below.

$$Minimize\ J(h) = \frac{1}{N}\sum_{i=1}^{N}(y_i - \hat{y}_i(h))^2$$

$$\begin{cases} u \in \{16, 32, 50, 64 \\ L \in \{1, 2, 3\} \\ o \in \{Adam, RMSprop, SGD\} \\ B \in \{16, 32, 64\} \\ E \in \{50, 100, 150\} \end{cases}$$

Pheromone trails are updated using a standard evaporation-reinforcement mechanism, expressed as follows:

$$\tau_{ij}{}^{(t+1)} = (1-\rho)\tau_{ij}{}^{(t)} + \sum_{k=1}^{n_{ants}} \frac{1}{f(X_k)+\varepsilon} \quad (2)$$

Where:

- $f(X_k)$ is the objective function value (or cost) of the solution X_k constructed by the k-th ant; a lower value of $f(X_k)$ results in a larger pheromone deposit.
- ε is a small positive constant (stability parameter) used to prevent division by zero and ensure numerical stability during the update process.

RNN-WOA Implementation

The control parameters adopted for the WOA in this study are summarized in Table 4. The WOA search is formulated as a constrained optimization problem, in which the objective functions in Equation 1 are minimized under the hyperparameter bounds specified below.

$$Minimize\ J(h) = \frac{1}{N}\sum_{i=1}^{N}(y_i - \hat{y}_i(h))^2$$

$$\begin{cases} u \in \{16, 32, 50, 64 \\ L \in \{1, 2, 3\} \\ o \in \{Adam, RMSprop, SGD\} \\ B \in \{16, 32, 64\} \\ E \in \{50, 100, 150\} \end{cases}$$

The position update of each whale is governed by a probability p, switching between a shrinking encircling mechanism and a spiral-shaped movement, expressed in Equation 3.

$$X(t+1) = \begin{cases} X^*(t) - A.|C.X^*(t) - X(t)| \ \ if\ p < 0.5\ and\ |A| < 1 \\ D'.\ e^{bl}.\cos(2\pi l) + X^*(t) \ \ if\ p \geq 0.5 \end{cases} \quad (3)$$

Table 2. Definition and search domains of RNN decision variables

Symbol	Hyperparameter	Definition	Search Domain
u	Hidden Units	Number of neurons in each recurrent layer	{16,32,50,64}
L	Layers	Total number of recurrent layers in the stack	{1,2,3}
o	Optimizer	The algorithm used to update weights	Adam
B	Batch Size	Number of samples processed before updating	{16,32,64}
E	Epochs	Number of complete passes through the dataset	{50,100,150}

Table 3. ACO control parameters

Parameter	Symbol	Value	Definition
Number of ants	n_{ants}	10	Number of candidate solutions (RNN configurations) evaluated per iteration
Number of iterations	n_{iter}	10	Maximum number of ACO iterations
Pheromone evaporation rate	ρ	0.4	Controls the rate at which pheromone trails decay to prevent premature convergence
Pheromone importance	α	1	Weight of pheromone trails in guiding the search process
Heuristic importance	β	2	Weight of solution quality in pheromone update
Initial pheromone value	τ_0	1.0	Initial pheromone level assigned uniformly to all decision variables.

Table 4. WOA control parameters

Parameter	Symbol	Value	Definition
Number of Whales	n_{whales}	10	Number of candidates RNN configurations evaluated per iteration.
Number of Iterations	n_{iter}	10	The maximum number of generational updates (100 total models).
Spiral Constant	b	1	Defines the shape of the logarithmic spiral movement.
Convergence Parameter	a	[2 → 0]	Linearly decreased from 2 to 0 to balance exploration and exploitation.
Probability Threshold	p	0.5	The switch between encircling and spiral mechanisms

3.3. Case Study

In their study, Koutous and Hilali [23] propose two formulations of the compressive stress-strain law for RE that apply to the ascending branch of the stress-strain curve. The general model (Equation 4) expresses stress as a quadratic function of strain, with parameters depending on the initial tangent modulus E_i and the secant modulus E_s. In the absence of detailed stiffness data, the authors also showed that for RE, a minimum value of $\theta = \frac{E_s}{E_i} = 0.5$ can be assumed, leading to a simplified parabolic law (Equation 5)

$$\sigma(\varepsilon) = E_s \varepsilon \left(1 - (1-\theta)\frac{\varepsilon}{\varepsilon_p}\right), \quad 0 \le \varepsilon \le \varepsilon_p \qquad (4)$$

$$\sigma(\varepsilon) = f_c \left[2\frac{\varepsilon}{\varepsilon_p} - \left(\frac{\varepsilon}{\varepsilon_p}\right)^2\right], \quad 0 \le \varepsilon \le \varepsilon_p \qquad (5)$$

Where σ is the compressive stress, ε is the axial strain, and f_c the compressive strength.

The simplified version of the formula proposed by Koutous and Hilali offers a simplified yet physically consistent method to describe the nonlinear stress development of RE up to peak strength. Unlike many previous studies that report stress-strain curves tied to specific mixtures or stabilization methods without providing transferable formulations, this model condenses the mechanical response into two parameters with explicit physical meaning: the peak compressive strength. f_c and the strain at peak stress ε_p.

This formulation is well-suited to probabilistic frameworks because it allows material variability to be propagated efficiently through explicitly defined random variables. In addition, the quadratic closed-form structure of the model provides strong numerical stability. This aspect is crucial in this study, since the constitutive law is treated as the reference model for training RNNs. At the same time, their hyperparameters are iteratively adjusted using ACO and WOA. The adoption of this formulation (Equation 5), therefore, anchors the predictive task to a compact and general constitutive model, which facilitates the systematic treatment of uncertainty and provides a reliable foundation for data-driven prediction of RE under compression stress.

To validate the proposed methodology, a numerical case study was performed to simulate the compressive mechanical response of URE. A probabilistic sampling strategy was employed to generate a synthetic dataset of 2,000 distinct stress-strain curves. This dataset was used consistently as the reference for both training and evaluating the Neural Networks across all optimization stages. For each realization, the constitutive behaviour followed the non-linear stress-strain relationship proposed by Koutous and Hilali (Equation 5).

For the purpose of constructing the training database, the parameters of the constitutive model were distinctively categorized into deterministic parameters and random variables. The specific statistical characterization assigned to these parameters, along with the selected values intended to represent the empirical variability of URE, are presented in the following subsections.

3.3.1. Deterministic Parameters

Axial Strain ε

In this study, the axial strain ε is distinctively treated as a deterministic input rather than a random variable. This choice is motivated by the nature of the experimental evidence and the modeling objectives. In mechanical characterization of RE, strain is typically controlled in laboratory tests, where specimens are compressed monotonically, and stress is recorded as a function of the imposed deformation. Accordingly, the variability in the response arises primarily from material properties such as the compressive strength. f_c and the strain at peak stress ε_p, rather than from the applied strain path itself. For this reason, the axial strain was treated as an imposed input. By treating axial strain as an imposed input, the probabilistic sampling process effectively explores the whole mechanical response domain while keeping the uncertainty concentrated on the governing intrinsic parameters (f_c ,ε_p).

Several studies in the literature have reported strain values for URE under compression, though with variability depending on soils, mixtures, and test specimens (Cylindrical, Prismatic, and Wallettes). Miccoli et al. [82] reported a mean vertical strain at one-third of the peak stress of 0.031%, reflecting the early deformation domain rather than the peak itself. Koutous and Hilali [23] provided values corresponding to the strain at maximum compressive strength, reporting averages of 0.81%, 0.95%, 0.92%, and 1.15% for raw-earth, sand-earth, rounded gravel-earth, and angular gravel-earth, respectively. Other studies, such as Gil-Martín et al. [14] and Bui and Morel [83], reported strain values at specimen rupture, close to 0.8%±0.1, and they also recorded 1.3%±0.1 for samples extracted from aged walls. By contrast, Ávila et al. [15] reported a peak strain of 3.4%, considerably higher than previous reported values. Overall, these studies reveal that some authors report strains at the point of maximum strength, while others extend to rupture strains at failure, which partly explains the range of values encountered.

Given the objective of defining a comprehensive input domain for predictive modeling, it is not necessary to retrieve every individual value reported in literature or attempt to extract values from stress-strain curves when they are not explicitly provided, as this process is often uncertain. Instead, the aim is to encompass both conservative lower bounds and the higher strain limits reported in recent research. This approach ensures that the database adequately reflects the

diversity of responses documented for URE. Crucially, the discretization of this range into ordered intervals establishes the sequential input structure required by the RNN, enabling the model to learn the path-dependent evolution of stress along the ascending branch of the constitutive curve, effectively characterizing the material's behavior from the initial loading stage up to failure. Accordingly, a practical evaluation range of 0.3% to 3.5% can be adopted. The specific sequence of axial strain values assessed in this study is presented in Table 5.

Table 5. Evaluated axial strain levels

Axial Strain value ε (%)	0.3	0.5	0.8	1	1.5	2	2.5	3	3.5

Table 6. Random variables: considered with associated probability distributions and statistical parameters

Random Variables		**Distribution**	**Mean Value**	**Coefficient of variation (COV) (%)**	**Standard deviation (%)**
f_c **(MPa)**	**Compressive Strength**	Lognormal	1.75	35	-
ε_p **(%)**	**Peak Strain**	Normal	1.9	-	0.8

3.3.2. Random Variables

Compressive Strength f_c

Compressive Strength of URE has been reported to vary significantly depending on soil composition, compaction, and testing. Ávila et al. [8] noted typical values between 1.0 and 2.5 MPa, with a few exceptions outside this range. To represent this variability within a probabilistic framework, f_c is modeled using a lognormal distribution, consistent with common practice for strength parameters which are strictly positive [84].

A mean value of 1.75 MPa, corresponding to the midpoint of the reported range, is adopted together with a Coefficient Of Variation (COV) of 35%, following the guidance of Kianfar and Toufigh [10]. This choice results in a distribution with a 95% probability interval approximately spanning 0.8-3.2 MPa, thereby covering the entire range reported in the literature while also accounting for potential scatter.

Peak Strain ε_p

Strain values reported in the literature for URE exhibit a wide dispersion. Most results concentrated between 0.8% and 1.2% [23, 83], though higher values such as 3.4% have also been recorded [15]. Other studies, such as [14], reported ultimate strain values close to 0.8%, which fall within the lower bound of this range. To the authors' knowledge, no previous study has explicitly treated peak strain as a random variable. Introducing this here provides a more realistic representation of material variability within a probabilistic framework. Accordingly, the peak strain is modelled using a normal distribution, with a mean value of 1.9%, corresponding to the midpoint of the 0.3-3.5% range derived from the literature, and a standard deviation of 0.8% is chosen so that approximately 95% of the simulated values fall within this interval.

A summary of the assessed random variables and their corresponding statistical parameters is presented in Table 6.

3.3.3. Model Implementation and Optimization Results

While the deterministic load protocol and stochastic material properties are completely specified, the numerical framework proceeds to implementation. When the runtime environment is booted up, at first, the synthetic data set of 2,000 stress-strain curves according to the distribution concepts detailed above (Table 6) is generated. After this internal data generation and partitioning, the post-processing becomes active, involving three-stage benchmarking.

With the configuration specified in Table 1, the Stage 1 Baseline model with its fixed hyperparameter is trained to create a performance baseline. The metaheuristic search loops for Stage 2 (ACO) and Stage 3 (WOA) are then started from the script.

There is only the same search space of hyperparameters and their degrees expressed in the methodology they both use, which consists of 10 agents over a population size for 10 iterations, leading to a consideration of already 100 different models over all possible combinations of the search space (324). The integrated workflow guarantees that the “ant” and “whale” optimization potential is compared against the baseline using precisely the same bright spots on image structures generated at run-time.

After those computational rounds are done, the prediction performance for each method is calculated. The final error metric is the MSE at this unseen 400-sample test. The performance comparison results were summarized in Table 7, which shows the best hyperparameters of each method and their corresponding error rates.

In order to gain more knowledge on the learning and search dynamics, visual representations over the training history between the baseline model and convergence trajectories of ACO and WOA algorithms are provided, as depicted in Figures 5, 6, and 7, respectively.

3.3.4. Experimental Validation Across Diverse URE Formulations

To evaluate the practical reliability and generalization capability of the proposed hybrid frameworks, an experimental validation was conducted using four distinct formulations of URE. These formulations include Raw Earth, Sand-Earth, Rounded Gravel-Earth, and Angular Gravel-Earth and are derived from the constitutive benchmarks established by Koutous and Hilali [23].

The main objective of this procedure is threefold:

- To assess the predictive fidelity of the RNN-ACO and RNN-WOA models across a diverse spectrum of physical properties.
- To quantify the performance enhancement achieved by the metaheuristic optimization of hyperparameters compared to a standard baseline RNN
- To evaluate the numerical stability of the models when subjected to varying grain size distributions and mineralogical compositions.

The mechanical characteristics of these formulations are summarized in Table 8, representing a broad range of compressive strengths and peak strains. The comparative results are illustrated in Figures 8, 9, 10, and 11. Each figure depicts the stress-strain curves of the URE formulations, contrasting the experimental reference data (derived from the validated constitutive model of Koutous and Hilali [23]) against the predictions generated by the baseline RNN, RNN-ACO, and RNN-WOA.

Table 7. Optimized hyperparameter configurations and final test set mean squared error for the baseline, ant colony optimization, and whale optimization algorithm models

Method	Optimal Hyperparameters (Units, Layers, Optimizer, Batch Size, Epochs)	Final Test MSE
Stage 1: Baseline RNN	(50, 1, Adam, 32, 50)	0.00049457
Stage 2: RNN-ACO	(16, 3, Adam, 16, 150)	0.00003937
Stage 3: RNN-WOA	(50, 3, RMSprop, 16, 150)	0.00006402

Table 8. Mechanical parameters and composition characteristics of the URE formulations used for experimental validation

URE Formulation	Compressive Strength f_c (MPa)	Peak Strain ε_p (%)
Raw Earth	1.95	0.81
Sand Earth	2.03	0.95
RoundedGravel-Earth	2.13	0.92
Angular Gravel-Earth	2.24	1.15

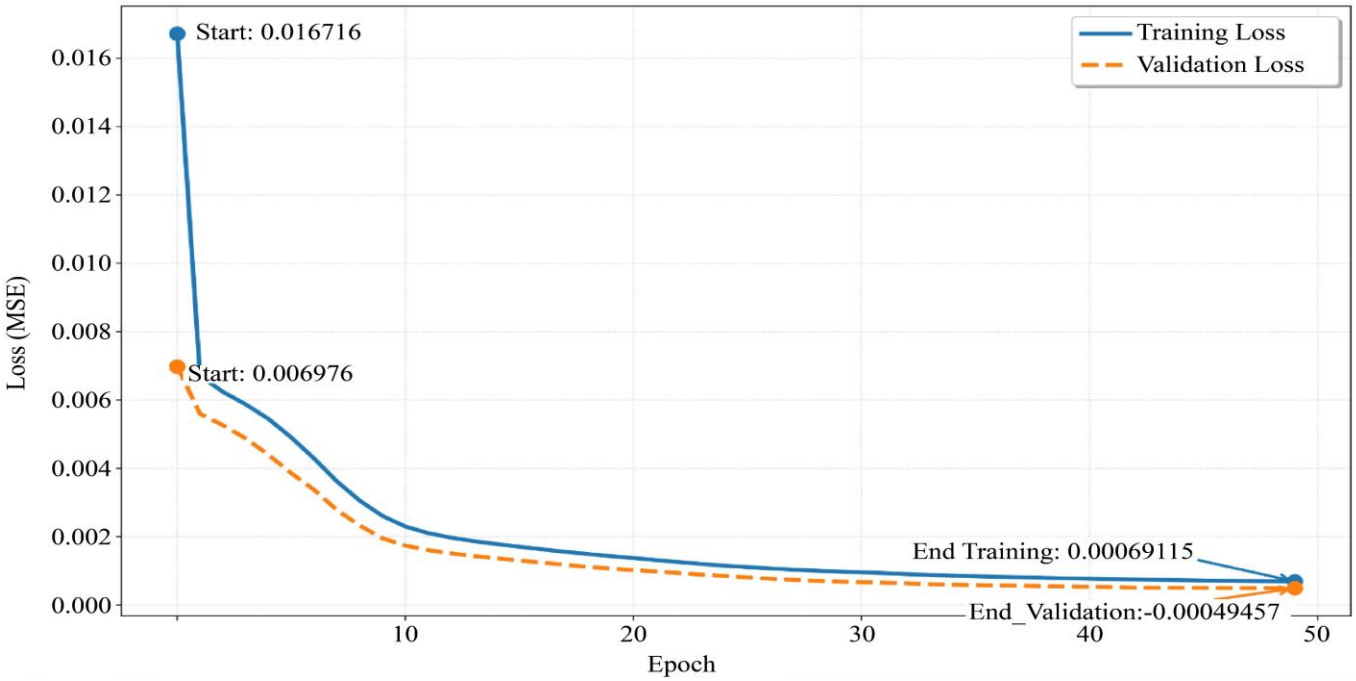

Fig. 5 Training loss (MSE) vs. Validation loss (MSE) for the manually-configured baseline model over the 50-epoch training duration

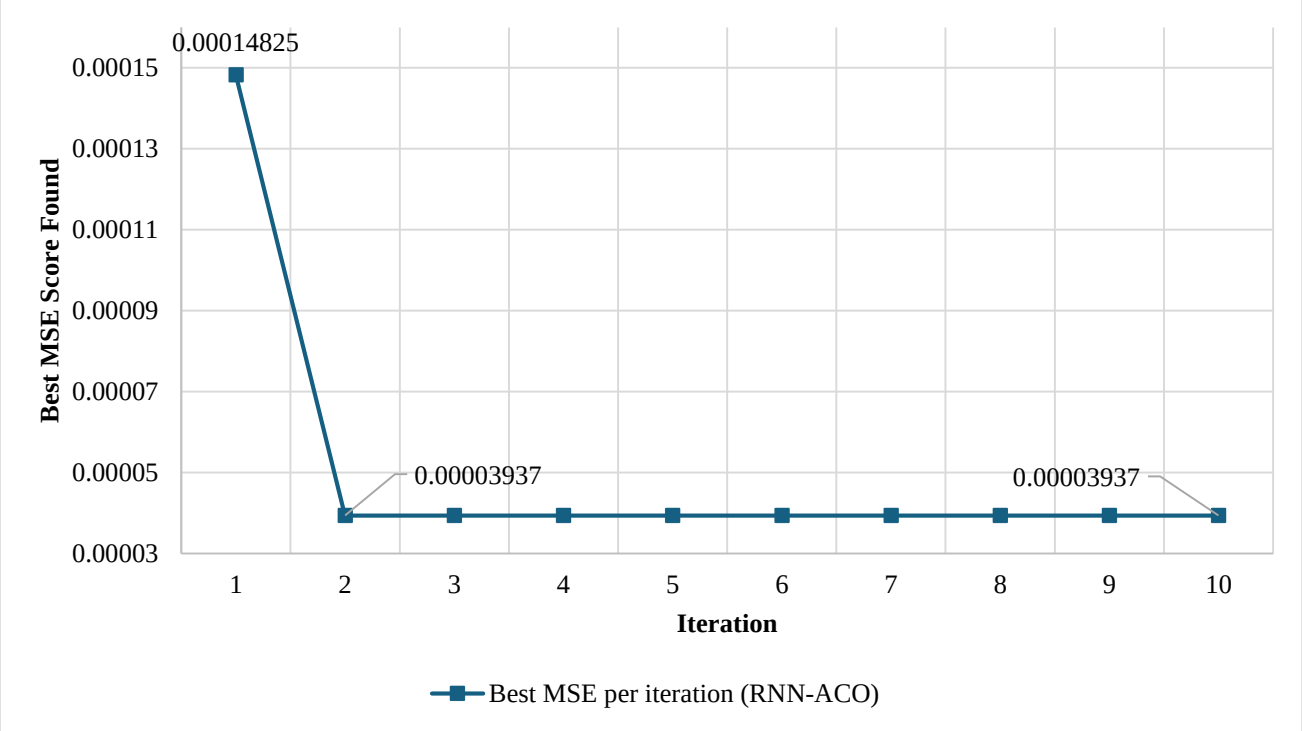

Fig. 6 Evolution of the best MSE score over 10 iterations of the Ant Colony Optimization (ACO) algorithm

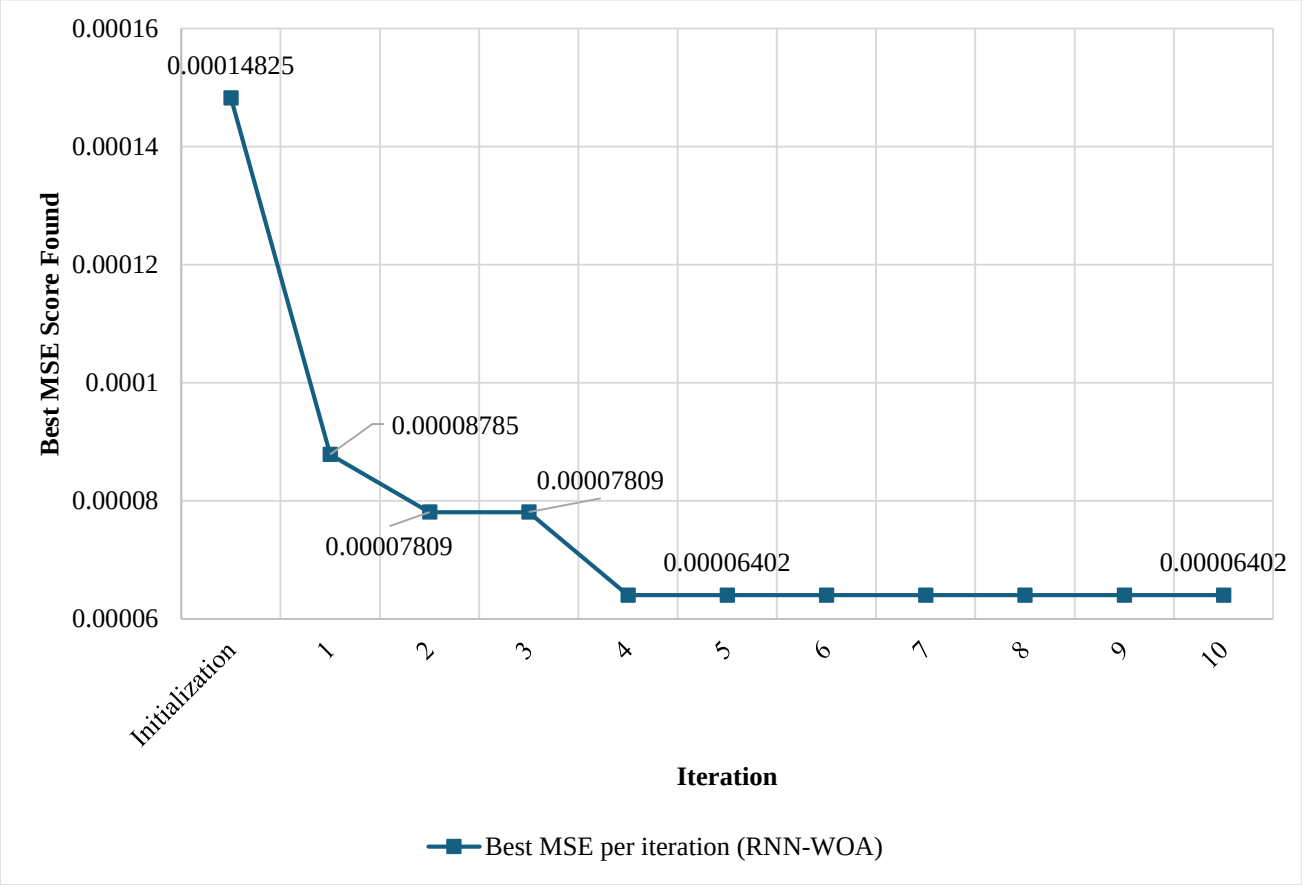

Fig. 7 Convergence plot for the Whale Optimization Algorithm (WOA) demonstrating its comparative optimization performance over 10 iterations

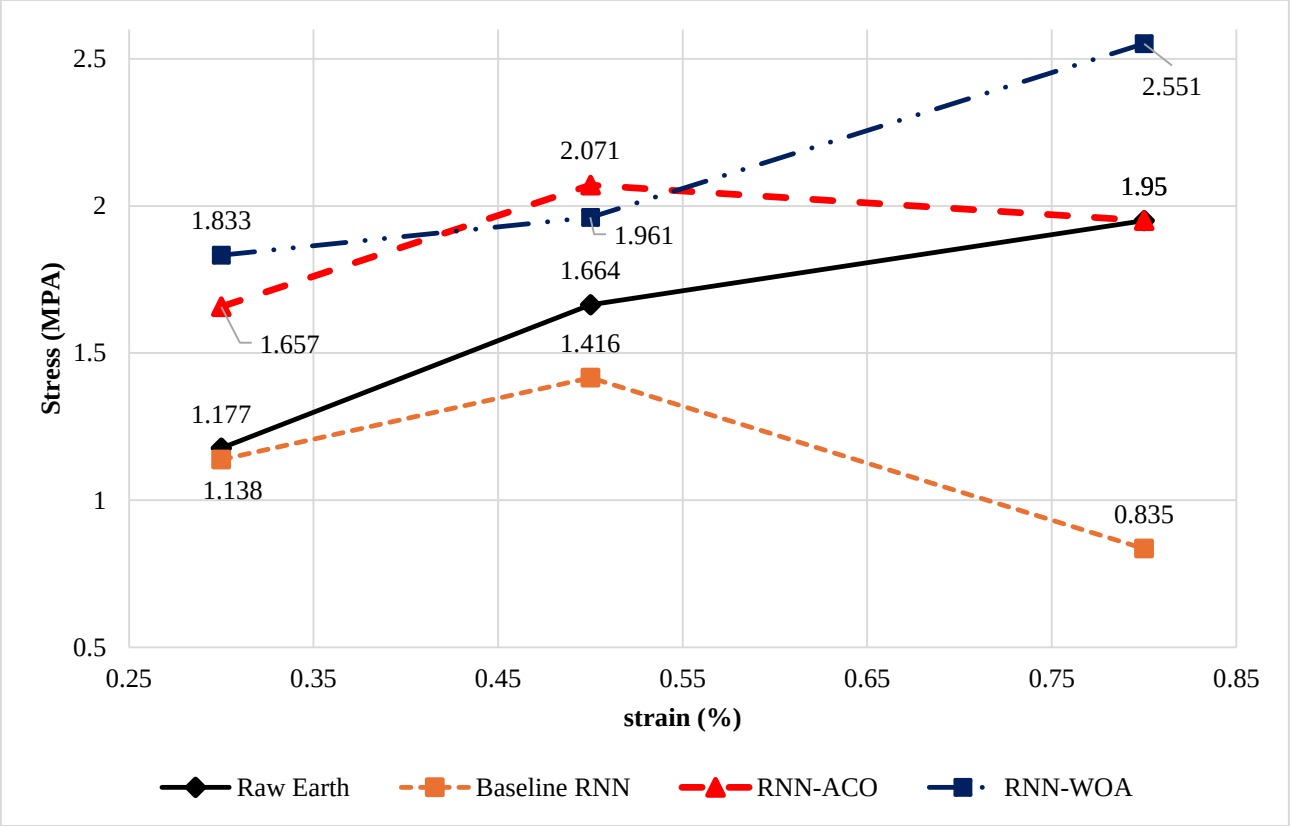

Fig. 8 Comparison of predicted and experimental stress-strain responses for raw earth

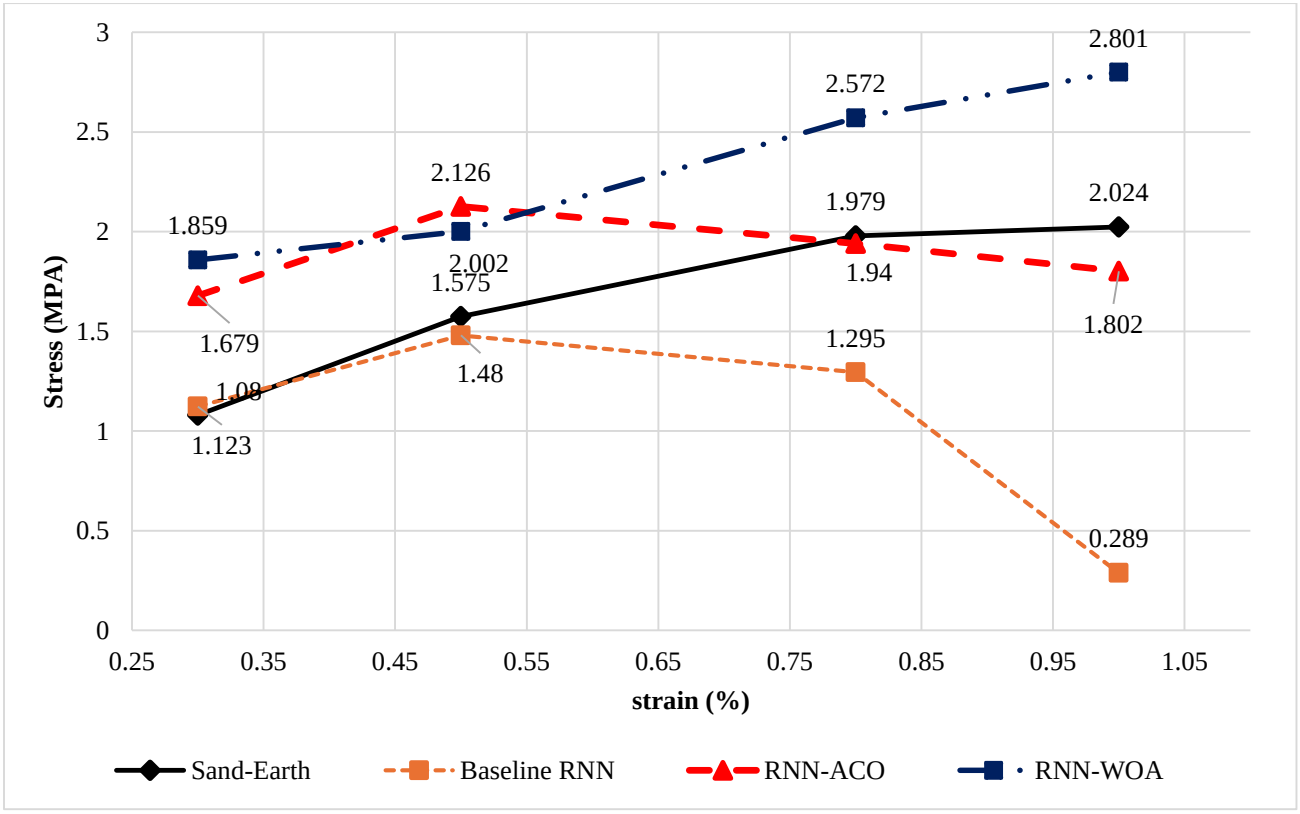

Fig. 9 Comparison of predicted and experimental stress-strain responses for sand-earth

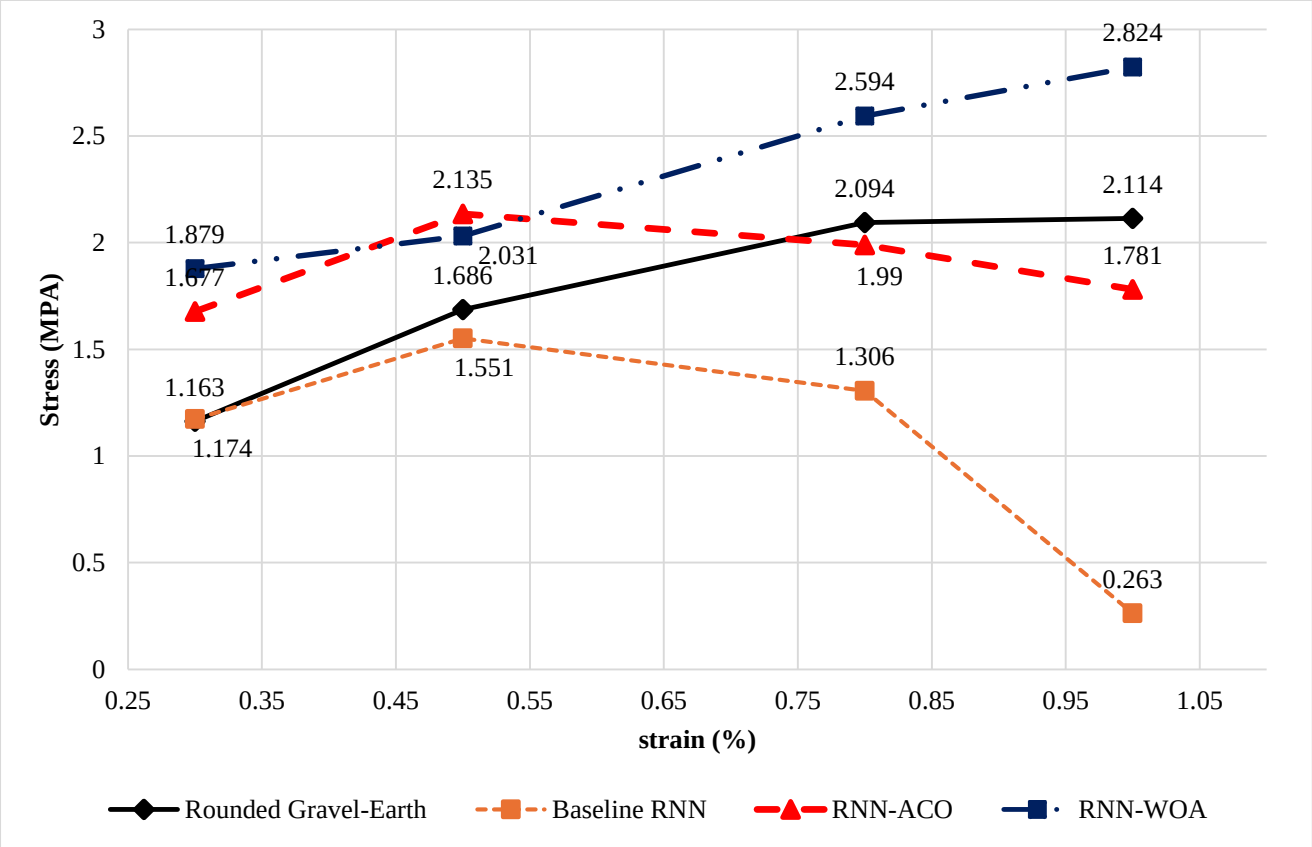

Fig. 10 Comparison of predicted and experimental stress-strain responses for rounded gravel-earth

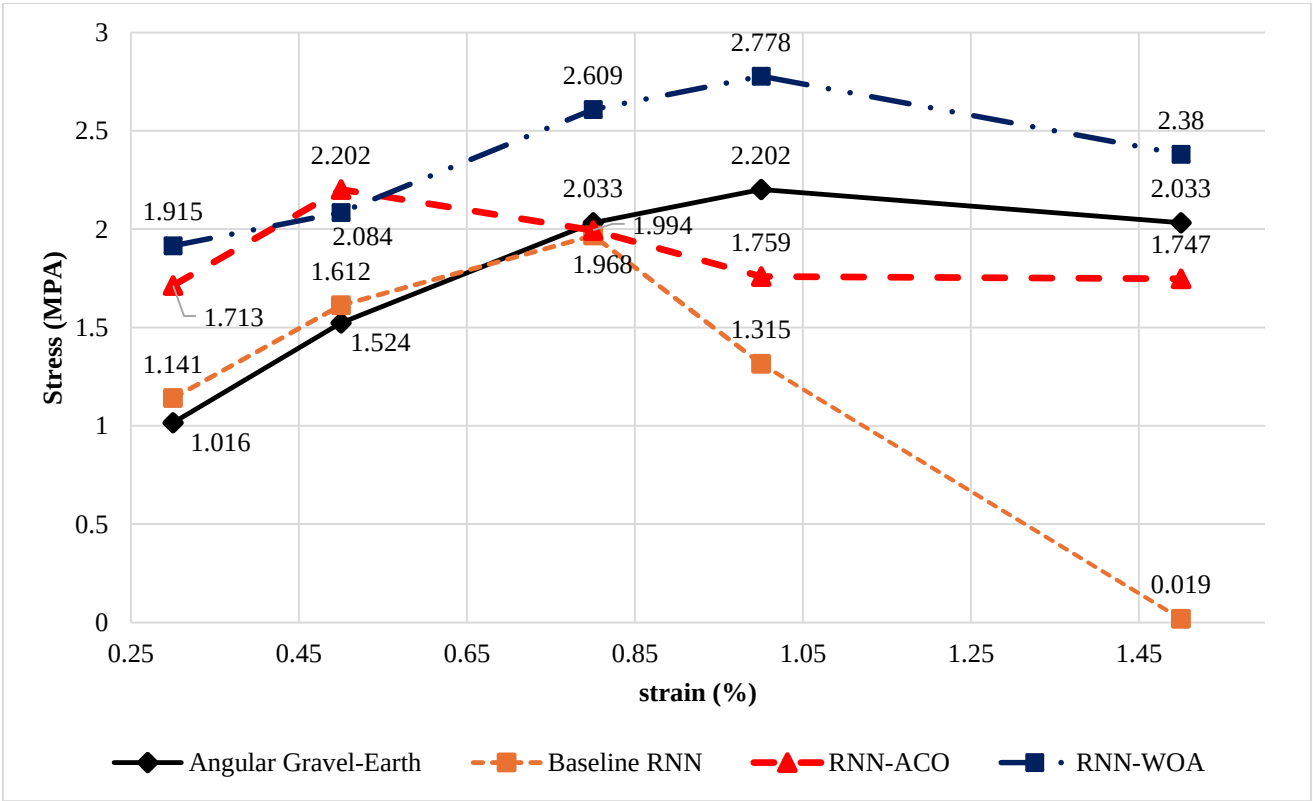

Fig. 11 Comparison of predicted and experimental stress-strain responses for angular gravel-earth

4. Discussion

Figure 5 illustrates the training and validation loss trajectories for the manually configured SimpleRNN model across 50 epochs. Both curves decline sharply during the initial training phase, indicating that the model rapidly learns fundamental temporal dependencies within the dataset. The close alignment between the training and validation loss curves throughout the training process indicates good generalization, with no evident signs of overfitting or divergence between the two.

The close correspondence between the training and validation loss curves during training suggests good generalization, as there is no overfitting or discrepancy between them. Around 15–20 epochs, the two losses converge and stop decreasing remarkably. This phenomenon indicates that, under the choice of hyperparameters made here, this represents the practical limit of what baseline configuration can express. It can be seen that one obtains a test MSE of 0.00049547, which serves as a descent baseline performance but implies the necessity for further fine-tuning in case higher precision is demanded.

Figure 6 shows the convergence curve of the ACO algorithm, indicating its ability to navigate the hyperparameter search space. Significant reduction at the beginning of optimization shows up in the best MSE, where the value drops fast from an initial 0.00014 to around 0.000039 in the second iteration. This prompt improvement suggests that ACO can rapidly identify promising areas of the neighborhoods containing near-optimal solutions. More than this, later changes are only of modest quality, indicating fast convergence and a nice future for learnability. This is further evidenced by the final test MSE of 0.00003937, which reflects a decrease in the baseline model of about 92%, thus underlining the importance of ACO-based hyperparameter tuning. The best architecture -with three layers of 16 units and a batch size of 16- implies that higher depth , along with a narrower architecture, is better than the initial design chosen manually for this dataset.

In the case of WOA, which is presented in Figure 7, a different optimization behavior is observed. Unlike ACO, WOA shows a slow and gradual reduction of MSE over the first four to five iterations until convergence. This algorithm eventually delivers better performance, but the size and pace of those gains are smaller. This behavior corresponds to a more conservative search, with 'less desperate' push into the hyperparameter space.

Test MSE of the best WOA-optimized model is 0.00006402, a level much lower than baseline but not superior to that obtained by ACO. However, this is an enhancement of around 87% compared to the RNN baseline, suggesting that WOA is still a promising optimizer, although it is not as efficient for the specific problem and dataset considered.

The ultimate comparison table (Table 7) summarizes the performance of the three modeling methods together. An interesting finding is the different architectural setups of the two algorithms. ACO converged to a shallow architecture with a smaller number of units, while WOA tended to have a higher number of units and an optimizer (RMSprop) or opponents. This discrepancy suggests that the search mechanisms of the two metaheuristics are involved differently in structuring this loss landscape. ACO's pheromone-driven random transitions seem more effective at obtaining compact, efficient architectures for this forecasting problem, and WOA's encircling-hunting mechanism leads to larger ones that provide decreasing returns.

The Neural Network structures used in other past studies on Earth and RE materials are compared with the approach proposed herein in Table 9. Previous studies have focused nearly exclusively on shallow ANN, mainly multi-layer perceptron with one hidden layer to model the static properties of mechanical performance or mix proportion optimization. These results consistently suggested that increasing the depth of a network would provide no significant better prediction performance and even might lead to overfitting in the case of small and heterogeneous datasets.

However, to the best of our knowledge, no existing work has exploited RNNs for RE and also combined these with metaheuristic optimization approaches such as ACO or WOA in this context. On the contrary, this study deals with a totally different modeling problem, which is capturing the nonlinear path-dependent stress-strain behavior of URE using RNN with ACO and WOA optimized hyperparameters. This comparison, on the one hand, proves that shallow networks can be sufficient to predict features of stationary properties; on the other hand, it shows that deep and/or recurrent models trained globally are needed when attempting to model complex time-dependent material responses, and this is also a methodological contribution.

Figures 8 through 11 present the experimental validation of the baseline RNN, RNN-ACO, and RNN-WOA models across the different URE formulations discussed in [23] and summarized in Table 8. Across all soil compositions, although the baseline RNN appears closer to the experimental curves at isolated strain levels, it consistently demonstrates poor generalization and severe numerical instability.

The baseline model typically underestimates stress and exhibits physically inconsistent degradation, particularly evident in the Angular Gravel-Earth case (Figure 11) after the 0.8% strain level. While the RNN-WOA framework maintains a more stable trajectory than the unoptimized RNN, it systematically overpredicts stress magnitudes, with the divergence from experimental benchmarks increasing with strain, thereby reducing physical fidelity in high-strength configurations.

Table 9. Comparative benchmark of deep learning architectures in moroccan structural engineering applications

Reference	Application	Optimal Architecture	Key Findings on Configuration
Belhaouate et al. [85]	Earth Construction	ANNs: 1 layer and 10 neurons	Shallow networks outperformed deeper ones by reducing complexity while maintaining accuracy.
Anysz and Narloch [45]	Cement Stabilized Rammed Earth mix design.	ANNs (Multi-Layer Perceptron) with 1 hidden layer, 6–13 neurons (optimal range)	Shallow single-hidden-layer networks achieved high prediction accuracy; increasing complexity did not significantly improve performance and risked overfitting.
Mustafa et al. [46]	Stabilized and Unstabilized Rammed Earth	ANN (Multi-Layer Perceptron), 1 hidden layer; 24 neurons (unstabilized soils); 41–44 neurons (stabilized soils); Levenberg–Marquardt algorithm, tanh activation	Shallow ANNs significantly outperformed multilinear regression**,** achieving very high accuracy (R^2 up to 0.988). Increasing model complexity beyond one hidden layer was unnecessary; optimal performance depended mainly on neuron count and input quality rather than depth.
This study	Unstabilized Rammed Earth	RNN with ACO optimized hyperparameters	Optimized deeper architectures (3 layers) combined with global search are required for complex time-series stress-strain paths.

In contrast, the RNN-ACO model exhibits the highest predictive fidelity and robustness across the entire validation suite. It accurately captures the nonlinear hardening behavior and stress magnitudes at low to intermediate strain levels while maintaining bounded, physically reasonable trends as the material approaches peak response. These results confirm that ACO in this case provides superior regularization and hyperparameter tuning for the RNN, effectively overcoming the stochastic instability of the unoptimized model and the overprediction tendencies of the WOA-optimized framework, resulting in a stable and high-fidelity predictive tool for complex URE compositions.

5. Conclusion

In this paper, the influence of metaheuristic hyperparameter optimization on the prediction accuracy of a SimpleRNN model to predict stress-strain behavior of RE material using the Koutous and Hilali [23] formula is investigated. The performance of baseline RNN is a reference point to assess the advantages achieved by optimization techniques, and evidently, both ACO and WOA dominate over it. ACO generates the most significant decrease in prediction error, whereas WOA is intermediate. These results demonstrate the strong potential of automated optimization strategies in improving the predictive capability of time-series models applied to nonlinear material behavior.

ACO showed a very rapid convergence and produced the lowest final MSE among all models tested. This shows that ACO is very efficient in exploring interesting parts of the hyperparameter search space with low computational cost. WOA also enhanced the model compared to baseline; however, its convergence was slower, and the final performance was just slightly less accurate. Collectively, both algorithms demonstrate that metaheuristic methods can identify hyperparameter combinations that would be hard to find manually and yet have a significant effect on forecast accuracy.

The experimental validation on four URE formulations, Raw Earth, Sand-Earth, Rounded Gravel-Earth, and Angular Gravel-Earth, also successfully proved the practical robustness of these optimized frameworks. Baseline RNN experienced an extreme numerical instability and captured no nonlinear hardening at significant strain levels, in contrast to the case of the high prediction fidelity and physical consistency over all soil compositions from RNN-ACO. This validation stage corroborates that the metaheuristic optimization integration, and ACO in particular here, is indeed able to regularize the learning process, allowing for stable and trustworthy predictions of URE behavior under real-world conditions.

Several future research opportunities spring from these results. The search space of hyperparameters in this work is kept restricted to some of the variables, such as the number of units. of layers, Batch size, Optimizer , and Number of training epochs, etc. In future work, the productivity of other hyperparameters, such as activation functions, regularization techniques, dropout rates, and various other recurrent cell

architectures, should be investigated. Other optimization algorithms, with Particle Swarm Optimization (PSO), Genetic Algorithm (GA), Bayesian Optimization (BO), or hybrid methods, among others, should also be investigated when they can give an additional improvement or faster convergence. Another significant generalization is to adopt different model types other than RNNs. Recent models like LSTM, GRU, 1DCNNs, Transformer-based architectures, or a hybrid of these can be used for better capturing temporal characteristics and, in turn, improve the prediction performance. By contrasting these alternatives, the question of which model families are most appropriate for modeling the mechanics of RE could be more completely addressed.

From a material science standpoint, the versatility of this method can be expanded as well. The models presented herein were exclusively trained on URE and in a limited strain range, thanks to the literature. In the future, it will be important to use materials data sets from a broader range of RE compositions, stabilizer contents, moisture content ranges, compaction energy levels, and construction modes. The treatment of the peak strain as a random variable is another limitation. The peak strain was considered a normal distribution because there were no data available. Despite the assumption-enabled modeling, future studies should provide more experimental data or explore different probability distributions in order to represent better the statistical behavior of peak strain in RE materials.

In conclusion, this research contributes valuable insights to the area of RE studies. It establishes that the AI-equipped machine learning models incorporating metaheuristic optimization can successfully reconstruct complex material behavior with high precision. Advanced prediction models will enable material design and structural performance assessment, and are a valuable tool for sustainable construction research. Given the generalized datasets, broader optimization schemes, and alternative model types that can be explored, this approach has significant potential for advancing both scientific understanding and practical applications of RE materials.

Funding Statement

This research was supported by the National Centre for Scientific and Technical Research (CNRST), Morocco, under the Excellence Research Fellowship Program.

References

[1] Daniel Maskell, Andrew Heath, and Pete Walker, "Comparing the Environmental Impact of Stabilisers for Unfired Earth Construction," *Key Engineering Materials*, vol. 600, pp. 132-143, 2014. [CrossRef] [Google Scholar] [Publisher Link]

[2] Deborah Arduin et al., "Life Cycle Assessment (LCA) in Earth Construction: A Systematic Literature Review Considering Five Construction Techniques," *Sustainability*, vol. 14, no. 20, pp. 1-30, 2022. [CrossRef] [Google Scholar] [Publisher Link]

[3] Ankita Yonzan et al., "Thermal Environment in Rammed Earth Structures: A Systematic Review on Thermal Comfort, Thermal Performance, and Climate Strategies," *Energy and Buildings*, vol. 349, 2025. [CrossRef] [Google Scholar] [Publisher Link]

[4] Liangyi Zhang, and Tiegang Zhou, "Experimental Study on the in-Plane Seismic Performance of Cement- and Polypropylene Fiber-Stabilized Rammed Earth Walls," *Journal of Building Engineering*, vol. 113, 2025. [CrossRef] [Google Scholar] [Publisher Link]

[5] Liangyi Zhang, and Tiegang Zhou, "Out-of-Plane Flexural Performance of Reinforced Rammed Earth Wall Panels," *Structures*, vol. 82, 2025. [CrossRef] [Google Scholar] [Publisher Link]

[6] Fernando Ávila et al., "Impact of Clay Content on the Fracture Behavior of Rammed Earth: Experimental and Nondestructive Assessment," *Construction and Building Materials*, vol. 501, pp. 1-11, 2025. [CrossRef] [Google Scholar] [Publisher Link]

[7] Rui A. Silva et al., "Evaluating the Seismic Behaviour of Rammed Earth Buildings from Portugal: From Simple Tools to Advanced Approaches," *Engineering Structures*, vol. 157, pp. 144-156, 2018. [CrossRef] [Google Scholar] [Publisher Link]

[8] Fernando Ávila, Esther Puertas, and Rafael Gallego, "Characterization of the Mechanical and Physical Properties of Unstabilized Rammed Earth: A Review," *Construction and Building Materials*, vol. 270, 2021. [CrossRef] [Google Scholar] [Publisher Link]

[9] J.D. Rodríguez-Mariscal, M. Solís, and Héctor Cifuentes, "Methodological Issues for the Mechanical Characterization of Unfired Earth Bricks," *Construction and Building Materials*, vol. 175, pp. 804-814, 2018. [CrossRef] [Google Scholar] [Publisher Link]

[10] Ehsan Kianfar, and Vahab Toufigh, "Reliability Analysis of Rammed Earth Structures," *Construction and Building Materials*, vol. 127, pp. 884-895, 2016. [CrossRef] [Google Scholar] [Publisher Link]

[11] Winston Lindqwister et al., "Predicting Compressive Stress-Strain Behavior of Elasto-Plastic Porous Media via Morphology-Informed Neural Networks," *Communications Engineering*, vol. 4, no. 1, pp. 1-12, 2025. [CrossRef] [Google Scholar] [Publisher Link]

[12] Hireballa Sangeetha, "Application of the Stress-Strain Curves for Concrete," *International Journal of Innovative Research in Computer Science & Technology (IJIRCST)*, vol. 10, Special Issue. 10, pp. 41-46, 2022. [Publisher Link]

[13] Youchao Zhang et al., "Properties of Sustainable Earth Construction Materials: A State-of-the-Art Review," *Sustainability*, vol. 16, no. 2, pp. 1-29, 2024. [CrossRef] [Google Scholar] [Publisher Link]

[14] Luisa María Gil-Martín, Manuel Alejandro Fernández-Ruiz, and Enrique Hernández-Montes, "Mechanical Characterization and Elastic Stiffness Degradation of Unstabilized Rammed Earth," *Journal of Building Engineering*, vol. 56, pp. 1-11, 2022. [CrossRef] [Google Scholar] [Publisher Link]

[15] Fernando Ávila et al., "Experimental and Numerical Evaluation of the Compressive and Shear Behavior of Unstabilized Rammed Earth," *Materials and Structures*, vol. 56, no. 7, pp. 1-14, 2023. [CrossRef] [Google Scholar] [Publisher Link]

[16] Quoc-Bao Bui et al., "Effect of Moisture Content on the Mechanical Characteristics of Rammed Earth," *Construction and Building Materials*, vol. 54, pp. 163-169, 2014. [CrossRef] [Google Scholar] [Publisher Link]

[17] Vasilios Maniatidis, and Peter Walker, "Structural Capacity of Rammed Earth in Compression," *Journal of Materials in Civil Engineering*, vol. 20, no. 3, pp. 230-238, 2008. [CrossRef] [Google Scholar] [Publisher Link]

[18] Abdelhakim El bourki, Ahmed Koutous, and Elmokhtar Hilali, "Date Palm Fiber-Reinforcement Impact on Rammed Earth Mechanical Behavior," *Construction and Building Materials*, vol. 461, 2025. [CrossRef] [Google Scholar] [Publisher Link]

[19] Satya Sai Deep Raavi, and Deb Dulal Tripura, "Compressive and Shear Behavior of Cement Stabilized Rammed Earth Wallettes Reinforced with Coir, Bamboo Splints and Steel Bars," *Structures*, vol. 53, pp. 1389-1401, 2023. [CrossRef] [Google Scholar] [Publisher Link]

[20] Fernando Ávila, Esther Puertas, and Rafael Gallego, "Mechanical Characterization of Lime-Stabilized Rammed Earth: Lime Content and Strength Development," *Construction and Building Materials*, vol. 350, 2022. [CrossRef] [Google Scholar] [Publisher Link]

[21] Lorenzo Miccoli et al., "Static Behaviour of Rammed Earth: Experimental Testing and Finite Element Modelling," *Materials and Structures*, vol. 48, no. 10, pp. 3443-3456, 2015. [CrossRef] [Google Scholar] [Publisher Link]

[22] Amirhossein Naseri et al., "Investigation of Mechanical Behavior of Slag-Stabilized Rammed Earth Reinforced by Carpet Polyacrylic Yarn Waste," *Scientific Reports*, vol. 15, no. 1, pp. 1-22, 2025. [CrossRef] [Google Scholar] [Publisher Link]

[23] A. Koutous, and E. Hilali, "Compression Stress-Strain Curve of Rammed Earth: Measuring and Modelling," *Results in Engineering*, vol. 18, pp. 1-16, 2023. [CrossRef] [Google Scholar] [Publisher Link]

[24] Shaoheng Guan, "*Machine Learning-based Constitutive Modelling for Granular Materials*," Doctoral E-Thesis, Swansea University, Wales, UK, 2024. [CrossRef] [Google Scholar] [Publisher Link]

[25] Tongming Qu et al., "Deep Learning Predicts Stress-Strain Relations of Granular Materials based on Triaxial Testing Data," *Computer Modeling in Engineering & Sciences*, vol. 128, no. 1, pp. 129-144, 2021. [CrossRef] [Google Scholar] [Publisher Link]

[26] S. Shajun Nisha, M. Mohamed Sathik, and M. Nagoor Meeral, *3 - Application, Algorithm, Tools Directly Related to Deep Learning*, Handbook of Deep Learning in Biomedical Engineering, Techniques and Applications, Academic Press, pp. 61-84, 2021. [CrossRef] [Google Scholar] [Publisher Link]

[27] Adam Wiemerslage, Kyle Gorman, and Katharina von der Wense, "Quantifying the Hyperparameter Sensitivity of Neural Networks for Character-level Sequence-to-Sequence Tasks," *Proceedings of the 18th Conference of the European Chapter of the Association for Computational Linguistics*, St. Julian's, Malta, pp. 674-689, 2024. [CrossRef] [Google Scholar] [Publisher Link]

[28] Wilfredo J. Puma-Villanueva, Eurípedes P. dos Santos, and Fernando J. Von Zuben, "A Constructive Algorithm to Synthesize Arbitrarily Connected Feedforward Neural Networks," *Neurocomputing*, vol. 75, no. 1, pp. 14-32, 2012. [CrossRef] [Google Scholar] [Publisher Link]

[29] Saman M. Almufti, *Metaheuristics Algorithms: Overview, Applications, and Modifications*, Deep Science Publishing, 2025. [CrossRef] [Google Scholar] [Publisher Link]

[30] Richard Fiifi Turkson et al., "Artificial Neural Network Applications in the Calibration of Spark-Ignition Engines: An Overview," *Engineering Science and Technology, an International Journal*, vol. 19, no. 3, pp. 1346-1359, 2016. [CrossRef] [Google Scholar] [Publisher Link]

[31] Naseem Alsadi, S. Andrew Gadsden, and John Yawney, "Intelligent Estimation: A Review of Theory, Applications, and Recent Advances," *Digital Signal Processing*, vol. 135, pp. 1-13, 2023. [CrossRef] [Google Scholar] [Publisher Link]

[32] Feifan Cheng, and Jinsong Zhao, "A Novel Process Monitoring Approach based on Feature Points Distance Dynamic Autoencoder," *Computer Aided Chemical Engineering*, vol. 46, pp. 757-762, 2019. [CrossRef] [Google Scholar] [Publisher Link]

[33] Pratima Kumari, and Durga Toshniwal, "Deep Learning Models for Solar Irradiance Forecasting: A Comprehensive Review," *Journal of Cleaner Production*, vol. 318, 2021. [CrossRef] [Google Scholar] [Publisher Link]

[34] E. N. Sanchez, *Appendix A - Artificial Neural Networks*, Neural Networks Modeling and Control, Applications for Unknown Nonlinear Delayed Systems in Discrete Time, Academic Press, pp. 117–124, 2020. [CrossRef] [Publisher Link]

[35] Krishna Devulapalli, "Neural Networks for Classification and Regression," *Biometrics & Biostatistics International Journal*, vol. 2, no. 6, pp. 183-185, 2015. [CrossRef] [Google Scholar] [Publisher Link]

[36] Pramod Kumar et al., *Analytical Statistics Techniques of Classification and Regression in Machine Learning*, Data Mining - Mehotds, Applications and Systems, 2020. [CrossRef] [Google Scholar] [Publisher Link]

[37] Juan Fernández et al., "Physics-Guided Recurrent Neural Network Trained with Approximate Bayesian Computation: A Case Study on Structural Response Prognostics," *Reliability Engineering & System Safety*, vol. 243, pp. 1-12, 2024. [CrossRef] [Google Scholar] [Publisher Link]

[38] Qingguo Yang et al., "Prediction of Mechanical Properties of Basalt Fiber Concrete using Hybrid Recurrent Neural Networks based on Freeze-Thaw Damage Quantification," *Journal of Building Engineering*, vol. 98, 2024. [CrossRef] [Google Scholar] [Publisher Link]

[39] Yukun Wang et al., "Recognition of Concrete Microcrack Images under Fluorescent Excitation based on Attention Mechanism Deep Recurrent Neural Networks," *Case Studies in Construction Materials*, vol. 20, pp. 1-18, 2024. [CrossRef] [Google Scholar] [Publisher Link]

[40] Meng Wu et al., "Seismic Performance Prediction of a Slope-Pile-Anchor Coupled Reinforcement System using Recurrent Neural Networks," *Engineering Geology*, vol. 338, pp. 1-31, 2024. [CrossRef] [Google Scholar] [Publisher Link]

[41] Tianyu Wang et al., "Seismic Response Prediction of Structures based on Runge-Kutta Recurrent Neural Network with Prior Knowledge," *Engineering Structures*, vol. 279, pp. 1-13, 2023. [CrossRef] [Google Scholar] [Publisher Link]

[42] Marina A. Maia et al., "Physically Recurrent Neural Network for Rate and Path-Dependent Heterogeneous Materials in a Finite Strain Framework," *Mechanics of Materials*, vol. 198, pp. 1-20, 2024. [CrossRef] [Google Scholar] [Publisher Link]

[43] Aryan Baibordy, Mohammad Yekrangnia, and Fatemeh Khodabakhshian, "Analysis of the Mechanical Behavior of Rammed Earth Mixes using Soft Computing Methods with an Emphasis on Sustainability," *The 1st International Conference on Net-Zero Civil Infrastructures: Innovations in Materials, Structures, and Management Practices (NTZR)*, Oslo, Norway, vol. 1, pp. 525-538, 2025. [CrossRef] [Google Scholar] [Publisher Link]

[44] Hubert Anysz et al., "Feature Importance of Stabilised Rammed Earth Components Affecting the Compressive Strength Calculated with Explainable Artificial Intelligence Tools," *Materials*, vol. 13, no. 10, pp. 1-20, 2020. [CrossRef] [Google Scholar] [Publisher Link]

[45] Hubert Anysz, and Piotr Narloch, "Designing the Composition of Cement Stabilized Rammed Earth using Artificial Neural Networks," *Materials*, vol. 12, no. 9, pp. 1-27, 2019. [CrossRef] [Google Scholar] [Publisher Link]

[46] Yassir Mubarak Hussein Mustafa et al., "Analysis of Unconfined Compressive Strength of Rammed Earth Mixes based on Artificial Neural Network and Statistical Analysis," *Materials*, vol. 15, no. 24, pp. 1-24, 2022. [CrossRef] [Google Scholar] [Publisher Link]

[47] Piotr Narloch et al., "Predicting Compressive Strength of Cement-Stabilized Rammed Earth based on SEM Images using Computer Vision and Deep Learning," *Applied Sciences*, vol. 9, no. 23, pp. 1-14, 2019. [CrossRef] [Google Scholar] [Publisher Link]

[48] Abdolhossein Hemmati-Sarapardeh et al., *Chapter 3 - Training and Optimization Algorithms*, Applications of Artificial Intelligence Techniques in the Petroleum Industry, pp. 51-78, 2020. [CrossRef] [Publisher Link]

[49] Christofer Larsson, *Chapter 5 - Optimization Techniques*, 5G Networks, Planning, Design and Optimization, Academic Press, pp. 103-122, 2018. [CrossRef] [Publisher Link]

[50] Hayati Mamur, Mehmet Ali Üstüner, and Mohammad Ruhul Amin Bhuiyan, "Future Perspective and Current Situation of Maximum Power Point Tracking Methods in Thermoelectric Generators," *Sustainable Energy Technologies and Assessments*, vol. 50, 2022. [CrossRef] [Google Scholar] [Publisher Link]

[51] Jesper Christensen, and Christophe Bastien, *Chapter | Seven - Heuristic and Meta-Heuristic Optimization Algorithms*, Nonlinear Optimization of Vehicle Safety Structures, Modeling of Structures Subjected to Large Deformations, pp. 277-314, 2016. [CrossRef] [Publisher Link]

[52] Christian Blum, "Ant Colony Optimization: A Bibliometric Review," *Physics of Life Reviews*, vol. 51, pp. 87-95, 2024. [CrossRef] [Google Scholar] [Publisher Link]

[53] Vinícius Moura Giglio, and Vladimir Guilherme Haach, "Optimization of Ultrasonic Tomography in Concrete using Non-Linear Paths through Bio-Inspired Algorithms," *NDT & E International*, vol. 152, 2025. [CrossRef] [Google Scholar] [Publisher Link]

[54] Zhengjie Zhan et al., "Multi-Objective Optimization in the Construction of Steel-Concrete Composite Columns with Carbon Emission Considerations: Pareto Front Development and Decision-Making," *Ain Shams Engineering Journal*, vol. 16, no. 2, pp. 1-21, 2025. [CrossRef] [Google Scholar] [Publisher Link]

[55] Yueer Zhou et al., "The Impact of Network Optimization on Airline Financial Performance: Evidence from China Domestic Routes," *Journal of Air Transport Management*, vol. 128, 2025. [CrossRef] [Google Scholar] [Publisher Link]

[56] Yang Yang et al., "Ant Colony-Inspired Cooperative Control of Multi- Magnetorheological Dampers System for Coupled Vibration Mitigation of Spatial Irregular Structures," *Engineering Structures*, vol. 334, 2025. [CrossRef] [Google Scholar] [Publisher Link]

[57] Sandeepan Roy, and Avijit Maji, "Metaheuristics-based Multistage Iterative Optimization Framework for Decomposed High-Speed Rail Systems Planning Problem," *Applied Soft Computing*, vol. 166, 2024. [CrossRef] [Google Scholar] [Publisher Link]

[58] Ahmed M. Ebid et al., "Ant Colony Optimization based Algorithm to Determine the Optimum Route for Overhead Power Transmission Lines," *Ain Shams Engineering Journal*, vol. 15, no. 1, pp. 1-12, 2024. [CrossRef] [Google Scholar] [Publisher Link]

[59] Phu-Anh-Huy Pham, and Nhat-Duc Hoang, "Metaheuristic Optimization of Extreme Gradient Boosting Machine for Enhanced Prediction of Lateral Strength of Reinforced Concrete Columns under Cyclic Loadings," *Results in Engineering*, vol. 24, pp. 1-18, 2024. [CrossRef] [Google Scholar] [Publisher Link]

[60] Chao Liu et al., "Improved Dynamic Adaptive Ant Colony Optimization Algorithm to Solve Pipe Routing Design," *Knowledge-Based Systems*, vol. 237, 2022. [CrossRef] [Google Scholar] [Publisher Link]

[61] Lei Xu et al., "Intelligent Planning of Fire Evacuation Routes using an Improved Ant Colony Optimization Algorithm," *Journal of Building Engineering*, vol. 61, 2022. [CrossRef] [Google Scholar] [Publisher Link]

[62] Marco Dorigo, Mauro Birattari, and Thomas Stutzle, "Ant Colony Optimization," *IEEE Computational Intelligence Magazine*, vol. 1, no. 4, pp. 28-39, 2006. [CrossRef] [Google Scholar] [Publisher Link]
[63] Christian Blum, "Ant Colony Optimization: Introduction and Recent Trends," *Physics of Life Reviews*, vol. 2, no. 4, pp. 353-373, 2005. [CrossRef] [Google Scholar] [Publisher Link]
[64] Seyedali Mirjalili, and Andrew Lewis, "The Whale Optimization Algorithm," *Advances in Engineering Software*, vol. 95, pp. 51-67, 2016. [CrossRef] [Google Scholar] [Publisher Link]
[65] Tansel Dokeroglu, Ayça Deniz, and Hakan Ezgi Kiziloz, "A Comprehensive Survey on Recent Metaheuristics for Feature Selection," *Neurocomputing*, vol. 494, pp. 269-296, 2022. [CrossRef] [Google Scholar] [Publisher Link]
[66] Quoc-Viet Pham et al., "Swarm Intelligence for Next-Generation Networks: Recent Advances and Applications," *Journal of Network and Computer Applications*, vol. 191, pp. 1-29, 2021. [CrossRef] [Google Scholar] [Publisher Link]
[67] Zulfiqar Ali Khan, and Izzatdin Abdul Aziz, "Dynamic OBL-Driven Whale Optimization Algorithm for Independent Tasks Offloading in Fog Computing," *High-Confidence Computing*, vol. 5, no. 4, pp. 1-13, 2025. [CrossRef] [Google Scholar] [Publisher Link]
[68] Fahui Miao et al., "Dynamic Multi-Swarm Whale Optimization Algorithm based on Elite Tuning for High-Dimensional Feature Selection Classification Problems," *Applied Soft Computing*, vol. 169, 2025. [CrossRef] [Google Scholar] [Publisher Link]
[69] Tibebu Bekele Shana et al., "Anomaly-based Intrusion Detection System based on SMOTE-IPF, Whale Optimization Algorithm, and Ensemble Learning," *Intelligent Systems with Applications*, vol. 27, pp. 1-18, 2025. [CrossRef] [Google Scholar] [Publisher Link]
[70] Biao He et al., "A Parameter-Adaptive Stochastic Resonance based on Whale Optimization Algorithm for Weak Signal Detection for Rotating Machinery," *Measurement*, vol. 136, pp. 658-667, 2019. [CrossRef] [Google Scholar] [Publisher Link]
[71] Iman Shafieenejad, "Maximizing the Velocity Deflection of Asteroid Didymos using the Whale Optimization Algorithm," *Planetary and Space Science*, vol. 258, 2025. [CrossRef] [Google Scholar] [Publisher Link]
[72] Keke Shi et al., "Integrated Hippopotamus and Whale Optimizations-based Impedance Control for Spacecraft Electromagnetic Separation," *Advances in Space Research*, 2025. [CrossRef] [Google Scholar] [Publisher Link]
[73] Wenjun Guo et al., "Whale Algorithm Optimized Anode Pressure Controller for Fuel Cell Systems in Ejector Recirculation Mode," *Energy and AI*, vol. 22, pp. 1-17, 2025. [CrossRef] [Google Scholar] [Publisher Link]
[74] Chunsheng Yu, "A Comprehensive Wind Power Prediction System based on Correct Multiscale Clustering Ensemble, Similarity Matching, and Improved Whale Optimization Algorithm-A Case Study in China," *Renewable Energy*, vol. 243, 2025. [CrossRef] [Google Scholar] [Publisher Link]
[75] Zhaoyu Zeng, and Fuyin Ni, "Research on the Optimal Scheduling Model of Energy Storage Plant based on Edge Computing and Improved Whale Optimization Algorithm," *Energy Engineering*, vol. 122, no. 3, pp. 1153-1174, 2025. [CrossRef] [Google Scholar] [Publisher Link]
[76] Farhad Soleimanian Gharehchopogh, and Hojjat Gholizadeh, "A Comprehensive Survey: Whale Optimization Algorithm and its Applications," *Swarm and Evolutionary Computation*, vol. 48, pp. 1-24, 2019. [CrossRef] [Google Scholar] [Publisher Link]
[77] Daniele Kauctz Monteiro et al., "Whale Optimization Algorithm for Structural Damage Detection, Localization, and Quantification," *Discover Civil Engineering*, vol. 1, no. 1, pp. 1-22, 2024. [CrossRef] [Google Scholar] [Publisher Link]
[78] Mohammad Rohani et al., "The Workflow Planning of Construction Sites using Whale Optimization Algorithm (WOA)," *The Turkish Online Journal of Design, Art and Communication*, vol. 6, pp. 2938-2950, 2016. [Google Scholar]
[79] Riham M. Ezzeldin, and Berge Djebedjian, "Optimal Design of Water Distribution Networks using Whale Optimization Algorithm," *Urban Water Journal*, vol. 17, no. 1, pp. 14-22, 2020. [CrossRef] [Google Scholar] [Publisher Link]
[80] Vivien Lai et al., "Investigating Dam Reservoir Operation Optimization using Metaheuristic Algorithms," *Applied Water Science*, vol. 12, no. 12, pp. 1-13, 2022. [CrossRef] [Google Scholar] [Publisher Link]
[81] Jherbyson Brito, and Letícia Miguel, "Optimization of a Reinforced Concrete Structure Subjected to Dynamic Wind Action," *Fracture and Structural Integrity*, vol. 16, no. 59, pp. 326-343, 2021. [CrossRef] [Google Scholar] [Publisher Link]
[82] Lorenzo Miccoli, Urs Müller, and Patrick Fontana, "Mechanical Behaviour of Earthen Materials: A Comparison between Earth Block Masonry, Rammed Earth and Cob," *Construction and Building Materials*, vol. 61, pp. 327-339, 2014. [CrossRef] [Google Scholar] [Publisher Link]
[83] Quoc-Bao Bui, and Jean-Claude Morel, "First Exploratory Study on the Ageing of Rammed Earth Material," *Materials*, vol. 8, no. 1, pp. 1-15, 2015. [CrossRef] [Google Scholar] [Publisher Link]
[84] Michael H. Faber, and John Dalsgaard Sørensen, "Reliability based Code Calibration," *The Joint Committee on Structural Safety*, pp. 1-17, 2002. [Google Scholar]
[85] Marouane Belhaouate, Mouna El Mkhalet, and Nouzha Lamdouar, "Artificial Neural Network-Based Prediction of Load-Bearing Capacity in Earthen Construction: A Comparative Analysis of Model Architectures In Morocco," *International Journal of Civil Engineering*, vol. 12, no. 9, pp. 49-50, 2025. [CrossRef] [Publisher Link]